ARTICLE

doi:10.1038/nature18600

A combinatorial strategy for treating KRAS-mutant lung cancer

Eusebio Manchado[1], Susann Weissmueller[1,2], John P. Morris IV[1], Chi-Chao Chen[1,3], Ramona Wullenkord[1], Amaia Lujambio[1,4], Elisa de Stanchina[5], John T. Poirier[5,6], Justin F. Gainor[7], Ryan B. Corcoran[7], Jeffrey A. Engelman[7], Charles M. Rudin[5,6], Neal Rosen[5,6] & Scott W. Lowe[1,8]

Therapeutic targeting of KRAS-mutant lung adenocarcinoma represents a major goal of clinical oncology. KRAS itself has proved difficult to inhibit, and the effectiveness of agents that target key KRAS effectors has been thwarted by activation of compensatory or parallel pathways that limit their efficacy as single agents. Here we take a systematic approach towards identifying combination targets for trametinib, a MEK inhibitor approved by the US Food and Drug Administration, which acts downstream of KRAS to suppress signalling through the mitogen-activated protein kinase (MAPK) cascade. Informed by a short-hairpin RNA screen, we show that trametinib provokes a compensatory response involving the fibroblast growth factor receptor 1 (FGFR1) that leads to signalling rebound and adaptive drug resistance. As a consequence, genetic or pharmacological inhibition of FGFR1 in combination with trametinib enhances tumour cell death *in vitro* and *in vivo*. This compensatory response shows distinct specificities: it is dominated by FGFR1 in KRAS-mutant lung and pancreatic cancer cells, but is not activated or involves other mechanisms in KRAS wild-type lung and KRAS-mutant colon cancer cells. Importantly, KRAS-mutant lung cancer cells and patients' tumours treated with trametinib show an increase in FRS2 phosphorylation, a biomarker of FGFR activation; this increase is abolished by FGFR1 inhibition and correlates with sensitivity to trametinib and FGFR inhibitor combinations. These results demonstrate that FGFR1 can mediate adaptive resistance to trametinib and validate a combinatorial approach for treating KRAS-mutant lung cancer.

KRAS encodes a GTPase that couples growth factor signalling to the MAPK cascade and other effector pathways. Oncogenic *KRAS* mutations compromise its GTPase activity, leading to accumulation of KRAS in the active GTP-bound state and thereby to hyperactive signalling that initiates and maintains tumorigenesis[1]. Owing to the high frequency of *KRAS* mutations in lung adenocarcinoma and other cancers, strategies to inhibit the KRAS protein or to exploit synthetic lethal interactions with a mutant *KRAS* gene have been widely pursued but have been fraught with technical challenges or produced inconsistent results[2–7]. Conversely, strategies to target key RAS effectors including MAPK pathway components RAF, MEK, and ERK have been hindered by toxicities associated with their sustained inhibition and/or adaptive resistance mechanisms[8–11].

Screen to identify trametinib sensitizers

Hypothesizing that sustained MAPK inhibition is necessary, but not sufficient, for targeting KRAS-mutant cancers, we performed a pool-based short hairpin RNA (shRNA) screen to identify genes whose inhibition sensitizes KRAS-mutant lung cancer cells to the FDA-approved MEK inhibitor trametinib (Supplementary Table 1). A customized short-hairpin RNA (shRNA) library targeting the human kinome was introduced into the TRMPVIN vector that we previously optimized for negative selection screening[12,13]. In this system, cassettes encoding a mir-30 shRNA linked to a dsRed fluorescent reporter are placed downstream of a tetracycline responsive promoter, enabling doxycycline dependent gene silencing and the facile tracking and/or sorting of shRNA expressing cells (Extended Data Fig. 1a)[12]. This library was transduced into H23 $KRAS^{G12C}$ mutant lung cancer cells expressing a reverse-tet-transactivator (rtTA3). The transduced populations were then treated with doxycycline in the presence or absence of 25 nM trametinib, a dose that effectively inhibits ERK signalling without substantially affecting proliferation (Extended Data Fig. 1b–e). After ten population doublings, changes in shRNA representation were determined by sequencing of shRNAs amplified from dsRed-sorted cells (Extended Data Fig. 1b).

As expected, shRNAs targeting essential genes (*RPA1* and *CDK11A*) were strongly depleted in both vehicle and trametinib-treated cells, whereas the relative representation of neutral non-targeting control shRNAs (*Renilla* (*REN*)) remained unchanged (Fig. 1a and Extended Data Fig. 1f, g). Using selection criteria that required an average four-fold or greater depletion between conditions, we identified 64 shRNAs corresponding to 53 genes that were selectively depleted upon MEK inhibition in trametinib-treated compared with untreated cells (Fig. 1a and Extended Data Fig. 1h). Of these, shRNAs targeting the eight genes for which multiple shRNAs identified as hits were validated using cell competition assays in multiple KRAS-mutant lung lines. These studies identified *BRAF*, *CRAF*, *ERK2*, and *FGFR1* as the top candidates in our screen (Fig. 1b and Extended Data Fig. 2a).

Trametinib has superior pharmacological properties compared with other MEK inhibitors because it impairs feedback reactivation of ERK[10]. Still, the fact that MAPK components were identified as hits in our screen implied that pathway reactivation eventually occurs. Indeed, although trametinib stably inhibits ERK signalling at 48 h—a time where rebound occurs with other agents[10]—we observed an increase in phospho-ERK after 6–12 days of drug exposure (Fig. 1c). This rebound was reduced by subsequently increasing

[1]Department of Cancer Biology and Genetics, Memorial Sloan Kettering Cancer Center, New York, New York 10065, USA. [2]Watson School of Biological Sciences, Cold Spring Harbor Laboratory, Cold Spring Harbor, New York 11724, USA. [3]Weill Cornell Graduate School of Medical Sciences, Cornell University, New York, New York 10065, USA. [4]Present address: Department of Oncological Sciences, Liver Cancer Program, Tisch Cancer Institute, Icahn School of Medicine at Mount Sinai, New York, New York 10029, USA. [5]Department of Molecular Pharmacology and Chemistry, Memorial Sloan Kettering Cancer Center, New York, New York 10065, USA. [6]Department of Medicine, Memorial Sloan Kettering Cancer Center, New York, New York 10065, USA. [7]Massachusetts General Hospital Cancer Center, Department of Medicine and Harvard Medical School, Boston, MA 02114, USA. [8]Howard Hughes Medical Institute, New York, New York 10065, USA.

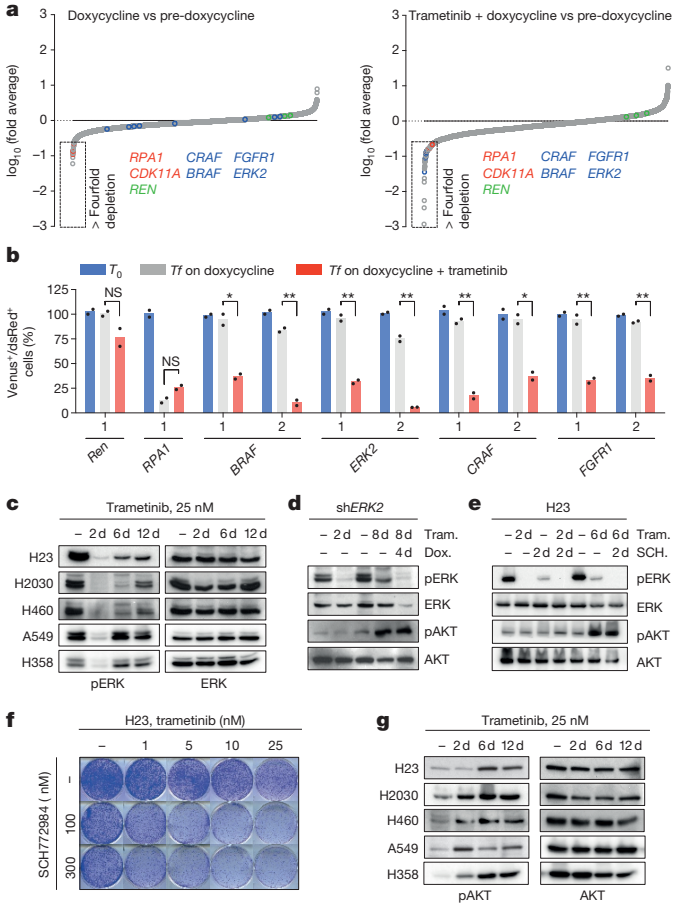

Figure 1 | Suppression of MAPK signalling effectors and FGFR1 sensitizes KRAS-mutant lung cells to trametinib. a, Relative abundance of each shRNA in the library in vehicle- or trametinib-treated H23 cells after ten population doublings on doxycycline. The mean of three (vehicle) and two (trametinib) replicates is plotted. Positive and negative controls included shRNAs targeting *RPA1* and *CDK11A* (red circles), and renilla (*REN*) luciferase (green circles). **b**, Quantification of fluorescent cells in competitive proliferation assays in H23 cells transduced with non-targeting control (*Ren*) or the indicated shRNAs. Data presented as mean ($n = 2$). $^*P < 0.05$, $^{**}P < 0.01$ (unpaired two-tailed *t*-test). **c**, Immunoblot of KRAS-mutant lung cells treated with 25 nM trametinib for various times. **d**, Immunoblot of H23 cells transduced with a doxycycline-inducible shRNA targeting *ERK2* and treated with trametinib (Tram.; 25 nM) and doxycycline (Dox.) for the times shown. **e**, Immunoblot of H23 cells treated with trametinib (25 nM), SCH772984 (500 nM), or a combination for the times shown. **f**, Clonogenic assay of H23 cells treated with trametinib, ERK inhibitor SCH772984, or a combination as indicated ($n = 3$). **g**, Immunoblot of KRAS-mutant lung cancer cells treated with 25 nM trametinib for various times. For gel source data, see Supplementary Fig. 1.

the concentration of trametinib, indicating that it is MEK dependent (Extended Data Fig. 2b). Accordingly, inducible knockdown of *ERK2*, *CRAF*, and *BRAF* blocked ERK signalling rebound and reduced clonogenic growth after trametinib treatment (Fig. 1d and Extended Data Fig. 2c, d). Similar effects were observed in KRAS-mutant lung cancer cells treated with trametinib and the ERK inhibitor SCH772984 (Fig. 1e, f and Extended Data Fig. 3)[14]. These observations emphasize the marked dependency of KRAS-mutant tumours on the MAPK signalling pathway.

In agreement with other studies, KRAS-mutant cells treated with trametinib also displayed compensatory activation of the PI3K and JAK/STAT pathways as assessed by AKT and STAT3 phosphorylation, respectively (Fig. 1d, e, g and Extended Data Figs 2c, 3b and 4a)[11,15]. Although the increase in STAT3 phosphorylation was transient (Extended Data Fig. 4a), AKT phosphorylation was sustained (Fig. 1g). In contrast to their effects on ERK signalling rebound, genetic or pharmacological inhibitions of MAPK signalling had little effect on the trametinib-induced increase in pAKT (Fig. 1d, e and Extended Data Figs 2c and 3b). The activation of multiple signalling pathways after trametinib treatment probably reflects a relief in pleiotropic feedback mechanisms produced by hyperactive RAS signalling in KRAS-mutant cells[8,9].

FGFR1 mediates adaptive drug resistance

Several RTKs have been implicated in adaptive resistance to RAS pathway antagonist[8,9,11,15–20]. The identification of *FGFR1* shRNAs as trametinib sensitizers raised the possibility that FGFR1 mediates MAPK and PI3K activation in trametinib-treated KRAS-mutant cells. In agreement, treatment of KRAS-mutant lung tumour cell lines with trametinib increased FGFR1 receptor and/or ligand expression together with FGFR pathway activation as assessed by an increase in phosphorylation of the FGFR adaptor protein FRS2 (Fig. 2a, b and Extended Data Figs 2b and 4b–e)[21]. In turn, FGFR1 activation correlated with an increase in the levels of RAS-GTP, phospho-AKT, and phospho-ERK (Fig. 2b and Extended Data Fig. 4e), which was prevented by FGFR1 knockdown (Fig. 2c). Accordingly, *FGFR1* shRNAs did not inhibit the proliferation of KRAS-mutant lung cancer, but displayed synergistic inhibitory effects when combined with trametinib (Fig. 2d, e and Extended Data Fig. 4f, g).

The combinatorial effects of FGFR1 inhibition and trametinib showed distinct specificities: for example, shRNAs targeting FGFR1 or FRS2, but not those targeting FGFR2 and 3, sensitized KRAS-mutant lung cancer cells to trametinib (Fig. 2f and Extended Data Fig. 4h, i). By contrast, FGFR1 knockdown had little impact on trametinib sensitivity in KRAS wild-type lung cancer cells (Fig. 2g). While *FGFR1* shRNAs synergized with trametinib in two KRAS-mutant pancreatic cancer cell lines, they showed little activity in trametinib-treated KRAS-mutant colorectal lines (Extended Data Fig. 5a). Importantly, this genotype and tissue specificity correlated with the ability of trametinib to trigger FRS2 phosphorylation when applied as a single agent (Extended Data Fig. 5b–d). Therefore, treatment of certain KRAS-mutant tumour types with trametinib induces a dependency on FGFR1 signalling that promotes adaptive drug resistance.

FGFR1 inhibition enhances trametinib effects

We next tested whether therapeutic strategies combining trametinib with an FGFR1 inhibitor could be effective in treating some KRAS-mutant lung cancers by combining trametinib with ponatinib, an FDA-approved multikinase inhibitor that inhibits FGFR1 and is being tested clinically for activity against FGFR1-amplified lung cancer (Extended Data Fig. 6a) (ref. 22 and https://clinicaltrials.gov/show/NCT01935336). Ponatinib had little effect on KRAS-mutant cells but countered the trametinib-induced increase in pFRS2, pERK, and pAKT, and synergized with trametinib in inhibiting cell proliferation (Fig. 3a–c, and Extended Data Fig. 6b–e). As observed in our genetic studies, this combination also showed combined activity in human KRAS-mutant pancreatic cancer cells and a *Kras*-mutant murine lung adenocarcinoma line (Extended Data Fig. 7a–c), but to a lesser extent in KRAS wild-type lung cancer cells or KRAS-mutant colon cancer cells (Fig. 3c). Although it remains possible that the synergistic effects of this combination involve the ability of ponatinib to target additional kinases, similar results were observed with two other chemically distinct FGFR inhibitors (Extended Data Figs 7d, e and 8a)[23,24]. Importantly, sensitivity to the combination of trametinib and FGFR inhibition correlated with the degree of pFRS2 induction after trametinib treatment (Extended Data Fig. 8b, c).

While our genetic and pharmacological studies establish the importance of the MAPK pathway in adaptive resistance to trametinib,

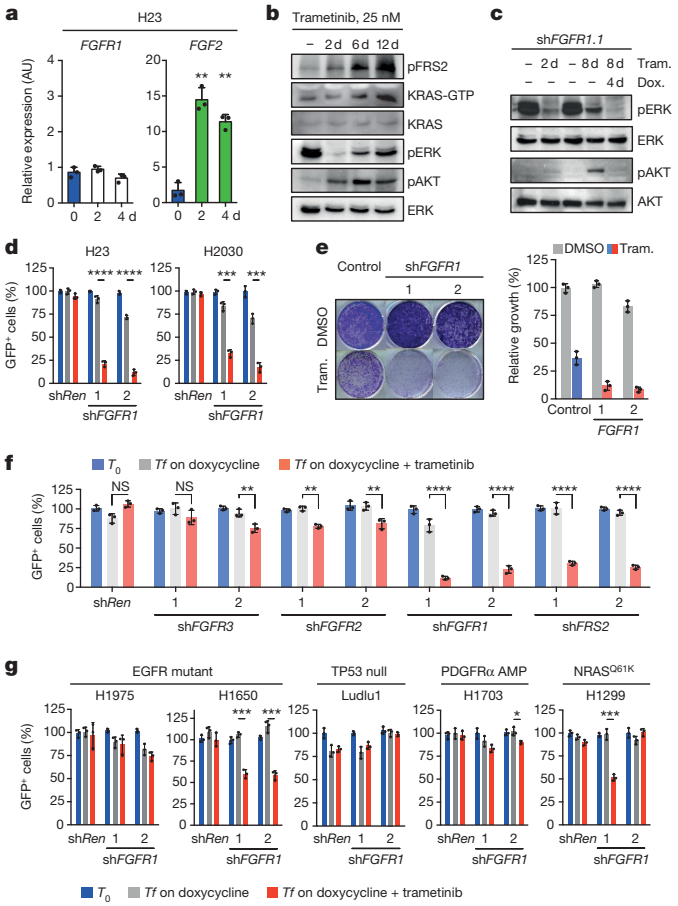

Figure 2 | Feedback activation of FGFR1 mediates adaptive resistance to trametinib in KRAS-mutant lung cells. a, Quantitative reverse transcription PCR (qRT–PCR) for *FGFR1* and *FGF2* in H23 cells treated with trametinib for the indicated times ($n = 3$). AU, arbitrary units. **b**, Immunoblot of H23 cells treated with 25 nM of trametinib for various times. **c**, Immunoblot of H23 cells transduced with a doxycycline-inducible shRNA targeting *FGFR1* and treated with trametinib (25 nM) and doxycycline for the times shown. **d**, Quantification of fluorescent cells in competitive proliferation assay in H23 and H2030 cells transduced with doxycycline-inducible non-targeting control (*Ren*) or *FGFR1* shRNAs ($n = 3$). **e**, Clonogenic assay of H23 cells transduced with *FGFR1* and non-targeting control shRNAs, and cultured with dimethylsulfoxide (DMSO) or trametinib (25 nM). Relative growth of DMSO- (grey bars) and trametinib-treated cells (blue and red bars) is shown (right) ($n = 3$). **f**, **g**, Quantification of fluorescent cells in competitive proliferation assays in H23 (**f**) and the indicated lung cancer cells (**g**) transduced with doxycycline-inducible non-targeting control (*Ren* (Renilla)) or the indicated shRNAs ($n = 3$). **a**, Paired two-tailed *t*-test. **d**, **f**, **g**, Unpaired two-tailed *t*-test. Data presented as mean ± s.d. $*P < 0.05$, $**P < 0.01$, $***P < 0.001$, $****P < 0.0001$. For gel source data, see Supplementary Fig. 1.

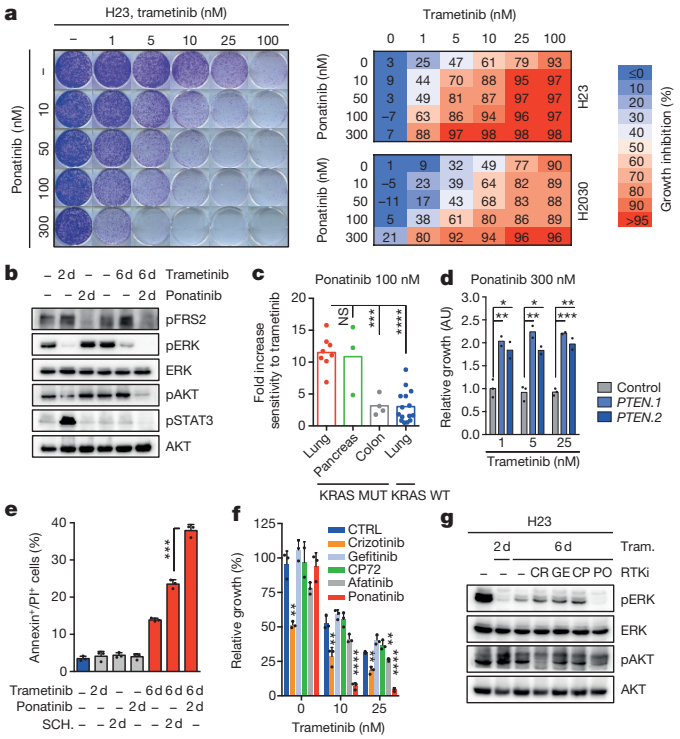

Figure 3 | Ponatinib synergizes with trametinib in inhibiting cell proliferation of KRAS-mutant lung cells. a, Clonogenic assay of H23 cells treated with trametinib, ponatinib, or their combination as indicated. Percentage inhibition at each concentration of the drugs in H23 and H2030 cells is presented (right). Data presented as mean of three independent experiments. **b**, Immunoblot of H23 cells treated with trametinib (25 nM), ponatinib (750 nM), or their combination for the times shown. **c**, Dot plot illustrating the sensitivity increase to trametinib after treatment with ponatinib (100 nM) in a panel of KRAS-mutant ($n = 15$) and KRAS wild-type ($n = 15$) cancer cell lines. Data presented as mean of two independent replicates. **d**, Quantification of the relative growth of H2030 cells transduced with *PTEN* and non-targeting control shRNAs, and treated with ponatinib (300 nM) in combination with trametinib (1, 5, and 25 nM). Data presented as mean of two independent replicates. **e**, Quantification of AnnexinV/PI double positive cells in H23 cells treated with trametinib (25 nM), ponatinib (300 nM), SCH772984 (1 μM), or their combination for the times shown ($n = 3$). **f**, Quantification of the relative growth of H23 cells treated with trametinib alone or in combination with 500 nM crizotinib, gefitinib, CP-724714, afatinib, or 300 nM ponatinib ($n = 3$). **g**, Immunoblot of H23 cells pre-treated with trametinib (25 nM) for 4 days, followed by treatment with trametinib (25 nM) alone or in combination with crizotinib (1 μM), gefitinib (1 μM), CP-724714 (1 μM), and ponatinib (750 nM) for 2 days. **c**–**f**, Unpaired two-tailed *t*-test. Error bars, mean ± s.d. $*P < 0.05$, $**P < 0.01$, $***P < 0.001$, $****P < 0.0001$. For gel source data, see Supplementary Fig. 1. Source Data for Fig. 3 are available in the online version of the paper.

we reasoned that the compensatory increase in PI3K/AKT signalling also plays a role and that its inhibition by ponatinib contributes to the effects of this drug combination. Accordingly, PTEN knockdown, which can increase PI3K signalling independently of RTK activation, promoted partial resistance to the drug combination in KRAS-mutant H2030 cells. This effect was not observed in H460 cells, a KRAS-mutant line that also harbours an activating mutation in the p110α catalytic subunit of PI3K (Fig. 3d and Extended Data Fig. 9a–c). Consistent with a role for PI3K signalling in promoting cell survival, co-treatment of H23 cells with trametinib and ponatinib triggered substantial apoptosis in a manner that was not observed after treatment with trametinib alone or in combination with an ERK inhibitor (Fig. 3e and Extended Data Fig. 9d). Thus, the combined ability of ponatinib to impact reactivation of the MAPK and PI3K pathways contributes to its combinatorial activity in KRAS-mutant lung cancer cells.

We also tested whether other RTKs known to be reactivated after MAPK inhibition contribute to adaptive resistance to trametinib in KRAS-mutant lung cancer cells[8,9,11,16–20,25,26]. While trametinib treatment of H23 and H2030 cells increased MET and ERBB2 (but not EGFR) levels (Extended Data Fig. 9e–g), inhibitors targeting these kinases did not synergize with trametinib under the conditions tested (Fig. 3f and Extended Data Figs 9h and 10a, b). Consistent with previous reports[11], the dual EGFR/ERBB2 inhibitor afatinib also showed combinatorial activity with trametinib in some KRAS-mutant lung cancer lines, although in our hands less robustly than the trametinib and ponatinib combination (Fig. 3f and Extended Data Figs 9h and 10a, b). Accordingly, none of the agents tested prevented the rebound in ERK signalling after trametinib treatment (Fig. 3g and

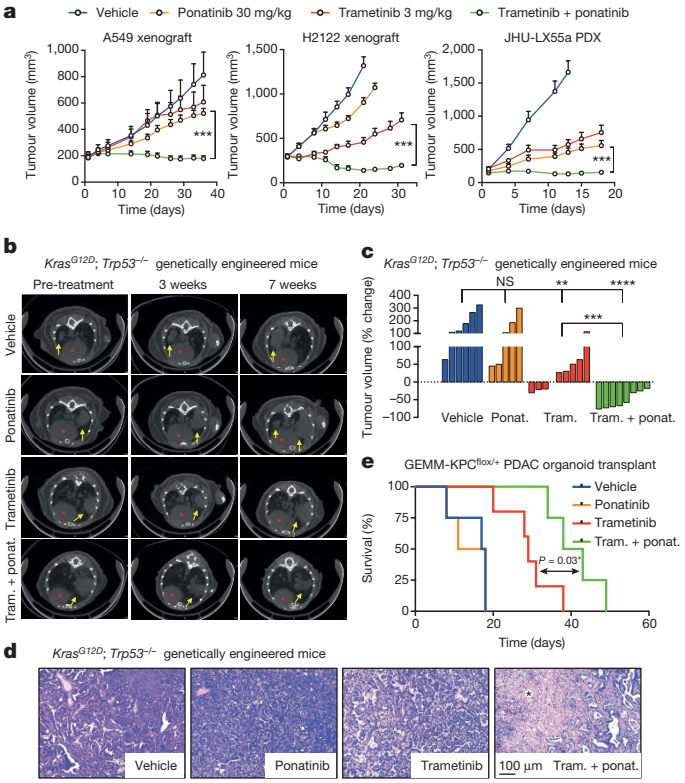

Figure 4 | Suppression of FGFR1 in combination with trametinib leads to regression of KRAS-mutant lung tumours. a, Tumour volumes of mice bearing A549 and H2122 xenografts, and JHU-LX55a patient-derived xenograft tumours and treated with vehicle, trametinib (3 mg/kg body weight), ponatinib (30 mg/kg body weight), or both drugs in combination for the indicated times. Error bars, mean ± s.e.m. ($n \geq 6$ per treatment group). **b**–**d**, Representative micro-computed tomography images of the lungs of $Kras^{G12D}$; $Trp53^{-/-}$ genetically engineered mice treated with vehicle, trametinib (3 mg/kg body weight), ponatinib (ponat.) (30 mg/kg body weight), or both drugs in combination for 3 and 7 weeks. Lung tumours are indicated by yellow arrows; red asterisks mark the hearts (**b**). A waterfall representation of the response for each tumour after 3 weeks of treatment is shown ($n \geq 5$ per group) (**c**). Representative haematoxylin and eosin stains are shown. Black asterisk indicates necrosis (**d**). **e**, Kaplan–Meier survival analysis of mice bearing pancreatic tumours resulting from orthotopic transplantation of GEMM-$KPC^{flox/+}$ PDAC organoids and treated as in **b** ($n \geq 4$ per group) (log-rank test). **a**, **c**, Unpaired two-tailed *t*-test. $*P < 0.05$, $**P < 0.01$, $***P < 0.001$, $****P < 0.0001$. Source Data for Fig. 4 are available in the online version of the paper.

Extended Data Fig. 10c, d). Thus, reactivation of FGFR1 signalling is a prominent mechanism of adaptive resistance to trametinib in KRAS-mutant lung cancer cells.

In vivo effects of MEK/FGFR1 inhibition

We validated our *in vitro* results in KRAS-mutant lung cancer xenografts, a KRAS-mutant patient-derived xenograft, and a genetically engineered mouse model (GEMM) of $Kras^{G12D}$-induced lung adenocarcinoma that accurately resembles the human disease[27]. A549 and H23 xenografts harbouring tet-responsive *FGFR1*- or control-shRNAs were treated with doxycycline and a daily dose of 3 mg/kg body weight of trametinib when tumours reached ~150 mm^3. While knockdown of FGFR1 or treatment with trametinib alone had only minor anti-tumour effects, the combination of FGFR1 knockdown with trametinib potently inhibited tumour growth and typically caused tumour regression (Extended Data Fig. 11a, b). Treatment of the xenografts, PDX and GEMM models with vehicle, trametinib, ponatinib, or the drug combination showed similar results, with only the combination producing marked tumour regressions despite no apparent toxicities (Fig. 4a–c and Extended Data Fig. 11c–e). Moreover, histological analysis of the residual tumour mass in GEMMs treated with the drug combination showed massive necrosis, an effect not seen with either agent alone (Fig. 4d). Similar results were observed in an organoid-based, transplantable model of $Kras^{G12D}$-driven pancreatic cancer, in which the drug combination produced marked cell death and significantly enhanced survival (Fig. 4e and Extended Data Fig. 11f).

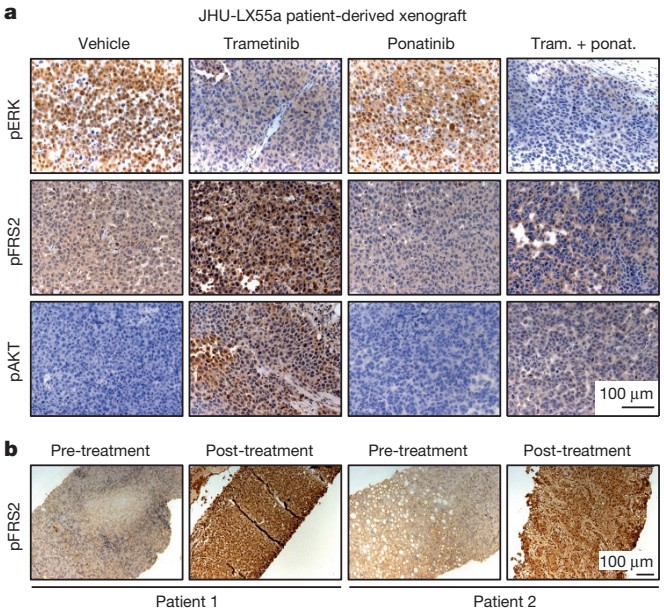

Figure 5 | Trametinib induces FGFR1 signalling in KRAS-mutant lung tumours. a, Tumour tissue from JHU-LX55a patient-derived xenografts treated with vehicle, trametinib (3 mg/kg body weight), ponatinib (30 mg/kg body weight), or both drugs in combination for 18 days was evaluated by IHC for phospho-FRS2, phospho-ERK, and phospho-AKT. **b**, Paired tumour biopsies from patients having KRAS-mutant lung adenocarcinomas (before and after treatment with the MEK inhibitor trametinib) were evaluated by IHC for phospho-FRS2.

We also examined the ability of trametinib to induce FGFR1 signalling in KRAS-mutant tumours. Consistent with *in vitro* results, a KRAS-mutant lung PDX model showed a concomitant increase in FRS2, ERK, and AKT phosphorylation after trametinib treatment—an effect that was cancelled by ponatinib (Fig. 5a and Extended Data Fig. 11g). Furthermore, FRS2 phosphorylation was dramatically increased after trametinib treatment in two patients with KRAS-mutant lung adenocarcinoma (Fig. 5b), indicating that the mechanism of adaptive resistance identified in our preclinical models is clinically relevant.

Discussion

In summary, by implementing a stringent approach for negative selection shRNA screening, we identified feedback activation of FGFR1 signalling as a prominent mechanism of adaptive resistance to the MEK inhibitor trametinib in KRAS-mutant lung cancer. The mechanism was specific: only shRNAs targeting *FGFR1*, but not other FGFR family members or other RTKs tested, conferred trametinib sensitivity, and only FGFR1 inhibition blocked compensatory reactivation of both ERK and AKT. In agreement, an unbiased ORF screen identified FGFR1, but not other RTKs, as sufficient to allow proliferation of KRAS-mutant colon cancer cells after KRAS suppression[28]. In our hands, the synergistic effects of the trametinib/FGFR inhibitor combinations were largely restricted to KRAS-mutant lung and pancreatic cancer cells, but not KRAS wild-type lung or KRAS-mutant colon cancer cells. These results strongly associate sensitivity to the combination with the magnitude of FRS2 phosphorylation after trametinib treatment alone and provide a mechanistic foothold to predict and study cell line and tumour variability.

Our results provide strong mechanistic support for combining trametinib with FGFR1 inhibitors for treating KRAS-mutant lung cancer and pinpoint a biomarker that might eventually be used to identify other patients likely to benefit from this drug combination. Although careful attention to additive or synergistic toxicities will be required for the clinical implementation of these findings, it seems likely that targeting a specific RTK such as FGFR1 will be more tolerable than targeting more pleiotropic factors such as AKT[29] and presents a rationale for developing more specific FGFR1 antagonists. Regardless, our study provides further evidence that targeting adaptive resistance mechanisms can improve the efficacy of molecular targeted therapies and provides one path towards developing rational strategies for treating KRAS-mutant lung cancer.

Online Content Methods, along with any additional Extended Data display items and Source Data, are available in the online version of the paper; references unique to these sections appear only in the online paper.

Received 23 November 2015; accepted 24 May 2016.
Published online 22 June 2016.

1. Downward, J. Targeting RAS signalling pathways in cancer therapy. *Nature Rev. Cancer* **3,** 11–22 (2003).
2. Ostrem, J. M., Peters, U., Sos, M. L., Wells, J. A. & Shokat, K. M. K-Ras(G12C) inhibitors allosterically control GTP affinity and effector interactions. *Nature* **503,** 548–551 (2013).
3. Barbie, D. A. *et al.* Systematic RNA interference reveals that oncogenic KRAS-driven cancers require TBK1. *Nature* **462,** 108–112 (2009).
4. Scholl, C. *et al.* Synthetic lethal interaction between oncogenic KRAS dependency and STK33 suppression in human cancer cells. *Cell* **137,** 821–834 (2009).
5. Luo, J. *et al.* A genome-wide RNAi screen identifies multiple synthetic lethal interactions with the Ras oncogene. *Cell* **137,** 835–848 (2009).
6. Stephen, A. G., Esposito, D., Bagni, R. K. & McCormick, F. Dragging ras back in the ring. *Cancer Cell* **25,** 272–281 (2014).
7. Cox, A. D., Fesik, S. W., Kimmelman, A. C., Luo, J. & Der, C. J. Drugging the undruggable RAS: mission possible? *Nature Rev. Drug Discov.* **13,** 828–851 (2014).
8. Lito, P., Rosen, N. & Solit, D. B. Tumor adaptation and resistance to RAF inhibitors. *Nature Med.* **19,** 1401–1409 (2013).
9. Samatar, A. A. & Poulikakos, P. I. Targeting RAS-ERK signalling in cancer: promises and challenges. *Nature Rev. Drug Discov.* **13,** 928–942 (2014).
10. Lito, P. *et al.* Disruption of CRAF-mediated MEK activation is required for effective MEK inhibition in KRAS mutant tumors. *Cancer Cell* **25,** 697–710 (2014).
11. Sun, C. *et al.* Intrinsic resistance to MEK inhibition in KRAS mutant lung and colon cancer through transcriptional induction of ERBB3. *Cell Reports* **7,** 86–93 (2014).
12. Zuber, J. *et al.* Toolkit for evaluating genes required for proliferation and survival using tetracycline-regulated RNAi. *Nature Biotechnol.* **29,** 79–83 (2011).
13. Manning, G., Whyte, D. B., Martinez, R., Hunter, T. & Sudarsanam, S. The protein kinase complement of the human genome. *Science* **298,** 1912–1934 (2002).
14. Morris, E. J. *et al.* Discovery of a novel ERK inhibitor with activity in models of acquired resistance to BRAF and MEK inhibitors. *Cancer Discov.* **3,** 742–750 (2013).
15. Lee, H. J. *et al.* Drug resistance via feedback activation of Stat3 in oncogene-addicted cancer cells. *Cancer Cell* **26,** 207–221 (2014).
16. Nazarian, R. *et al.* Melanomas acquire resistance to B-RAF(V600E) inhibition by RTK or N-RAS upregulation. *Nature* **468,** 973–977 (2010).
17. Villanueva, J. *et al.* Acquired resistance to BRAF inhibitors mediated by a RAF kinase switch in melanoma can be overcome by cotargeting MEK and IGF-1R/PI3K. *Cancer Cell* **18,** 683–695 (2010).
18. Corcoran, R. B. *et al.* EGFR-mediated re-activation of MAPK signaling contributes to insensitivity of BRAF mutant colorectal cancers to RAF inhibition with vemurafenib. *Cancer Discov.* **2,** 227–235 (2012).
19. Prahallad, A. *et al.* Unresponsiveness of colon cancer to BRAF(V600E) inhibition through feedback activation of EGFR. *Nature* **483,** 100–103 (2012).
20. Duncan, J. S. *et al.* Dynamic reprogramming of the kinome in response to targeted MEK inhibition in triple-negative breast cancer. *Cell* **149,** 307–321 (2012).
21. Kouhara, H. *et al.* A lipid-anchored Grb2-binding protein that links FGF-receptor activation to the Ras/MAPK signaling pathway. *Cell* **89,** 693–702 (1997).
22. Gozgit, J. M. *et al.* Ponatinib (AP24534), a multitargeted pan-FGFR inhibitor with activity in multiple FGFR-amplified or mutated cancer models. *Mol. Cancer Ther.* **11,** 690–699 (2012).
23. Guagnano, V. *et al.* Discovery of 3-(2,6-dichloro-3,5-dimethoxy-phenyl)-1-{6-[4-(4-ethyl-piperazin-1-yl)-phenylamino]-pyrimidin-4-yl}-1-methyl-urea (NVP-BGJ398), a potent and selective inhibitor of the fibroblast growth factor receptor family of receptor tyrosine kinase. *J. Med. Chem.* **54,** 7066–7083 (2011).
24. Gavine, P. R. *et al.* AZD4547: an orally bioavailable, potent, and selective inhibitor of the fibroblast growth factor receptor tyrosine kinase family. *Cancer Res.* **72,** 2045–2056 (2012).
25. Li, F. *et al.* FGFR-mediated reactivation of MAPK signaling attenuates antitumor effects of imatinib in gastrointestinal stromal tumors. *Cancer Discov.* **5,** 438–451 (2015).
26. Traer, E. *et al.* Ponatinib overcomes FGF2-mediated resistance in CML patients without kinase domain mutations. *Blood* **123,** 1516–1524 (2014).
27. Jackson, E. L. *et al.* The differential effects of mutant p53 alleles on advanced murine lung cancer. *Cancer Res.* **65,** 10280–10288 (2005).
28. Shao, D. D. *et al.* KRAS and YAP1 converge to regulate EMT and tumor survival. *Cell* **158,** 171–184 (2014).
29. Shimizu, T. *et al.* The clinical effect of the dual-targeting strategy involving PI3K/AKT/mTOR and RAS/MEK/ERK pathways in patients with advanced cancer. *Clin. Cancer Res.* **18,** 2316–2325 (2012).

Supplementary Information is available in the online version of the paper.

Acknowledgements We thank M. Sánchez-Céspedes, R. Somwar, and H. Varmus for sharing cell lines; S. Tian, J. Ahn, M. Taylor, A. Shroff, and J. Plevy for technical assistance; C. J. Sherr, L. E. Dow, P. Lito, T. Kastenhuber, and J. Leibold for advice on experimental design and/or for editing the manuscript; and other members of the Lowe laboratory for advice and discussions. This work was supported by a program project grant from the National Cancer Institute (S.W.L., N.R.), a grant from the Center of Experimental Therapeutics (S.W.L., N.R.), a Stand Up To Cancer grant from the American Association for Cancer Research (N.R., J.A.E., C.R.), and a Cancer Center Support grant to MSKCC. E.M. was supported by The Jane Coffin Childs Memorial Fund for Medical Research and a K99/R00 grant from the National Institutes of Health/National Cancer Institute. S.W. was supported by the Annette Kade Fellowship from the Watson School of Biological Sciences. R.W. was supported by a Carl-Duisberg Fellowship from the Bayer Foundation. A.L. was supported by an EMBO Long-Term fellowship. E.d.S. received support through the Geoffrey Beene Cancer Research Center. S.W.L. is the Geoffrey Beene Chair of Cancer Biology and a Howard Hughes Medical Institute investigator.

Author Contributions E.M. conceived the project, performed and analysed experiments, and wrote the paper with assistance of all authors. S.W., C.C., and R.W. performed and analysed *in vitro* experiments. S.W., J.P.M., and E.d.S. performed and analysed *in vivo* experiments. A.L. helped design and produce the shRNA library. J.T.P. and C.R. provided and analysed patient-derived xenografts. J.F.G., R.B.C., and J.A.E. provided human specimens. N.R. conceived the project, supervised experiments, and wrote the paper. S.W.L. conceived the project, supervised experiments, analysed data, and wrote the paper.

Author Information Reprints and permissions information is available at www.nature.com/reprints. The authors declare competing financial interests: details are available in the online version of the paper. Readers are welcome to comment on the online version of the paper. Correspondence and requests for materials should be addressed to N.R. (rosenn@mskcc.org) or S.W.L. (lowes@mskcc.org).

Reviewer Information *Nature* thanks J. Tyner and the other anonymous reviewer(s) for their contribution to the peer review of this work.

METHODS

Pooled negative-selection RNA interference screening. A custom shRNA library targeting 526 human kinases was designed using miR30-adapted DSIR predictions refined with 'sensor' rules[30] (six shRNAs per gene) and constructed by PCR-cloning a pool of oligonucleotides synthesized on customized arrays (Agilent Technologies and CustomArray) as previously described (Supplementary Table 1)[12]. The list of genes was obtained from the KinBase Database (http://kinase.com/human/kinome/) and was manually curated. After sequence verification, 3,156 shRNAs (5–6 per gene) were combined with 20 positive- and negative-control shRNAs at equal concentrations in one pool. This pool was subcloned into the TRMPV-Neo vector and transduced in triplicates into Tet-on H23 KRAS-mutant lung cancer cells using conditions that predominantly led to a single retroviral integration and represented each shRNA in a calculated number of at least 1,000 cells. Transduced cells were selected for 6 days using 1 mg ml^{-1} G418 (Invitrogen); at each passage more than 30 million transduced cells were maintained to preserve library representation throughout the experiment. After drug selection, T_0 samples were obtained (~30 million cells per replicate ($n = 3$)) and cells were subsequently cultured in the presence or absence of trametinib (25 nM) and 1 μg ml^{-1} doxycycline to induce shRNA expression. After ten population doublings (*Tf*), about 15 million shRNA-expressing (dsRed$^+$/Venus$^+$) cells were sorted for each replicate using a FACSAriaII (BD Biosciences). Genomic DNA from T_0 and *Tf* samples was isolated by two rounds of phenol extraction using Phase Lock tubes (5 Prime) followed by isopropanol precipitation. Deep-sequencing template libraries were generated by PCR amplification of shRNA guide strands as previously described[12]. Libraries were analysed on an Illumina Genome Analyzer at a final concentration of 8 pM; 50 nucleotides of the guide strand were sequenced using a custom primer (miR30EcoRISeq, TAGCCCCTTGAATTCCGAGGCAGTAGGCA). To provide a sufficient baseline for detecting shRNA depletion in experimental samples, we aimed to acquire >500 reads per shRNA in the T_0 sample, which required more than 20 million reads per sample to compensate for disparities in shRNA representation inherent to the pooled plasmid preparation or introduced by PCR biases. With these conditions, we acquired T_0 baselines of >500 reads for 3,151 (97.9%) shRNAs. Sequence processing was performed using a customized Galaxy platform[31].

Using selection criteria that required an shRNA depletion averaging greater than fourfold after ten population doublings and an effect greater than fourfold in trametinib-treated cells with respect to untreated ones, 64 shRNAs were identified. The eight targets for which at least two shRNAs were selectively depleted after trametinib treatment were subject to secondary validation in cell competition assays using multiple KRAS-mutant lung cancer cell lines. Six targets validated in the cell line in which the primary screen was performed (H23 cells) and four (*BRAF*, *CRAF*, *ERK2*, and *FGFR1*) across a panel of KRAS-mutant lung cancer cells; as such, these represented the top hits of our screen.

Plasmids and recombinant proteins. All vectors were derived from the Murine Stem Cell Virus (MSCV, Clontech) retroviral vector backbone. miR30- and mirE-based shRNAs were designed and cloned as previously described[12] and sequences are available in Supplementary Table 1. shRNAs were cloned into the TRMPV-Neo (pSIN-TREdsRed-miR30-PGK-Venus-IRES-NeoR), LT3GEPIR (TRE3G-GFP-miRE-PGK-PuroR-IRES-rtTA3), and MLP (LTR-miR30-PGK-PuroR-IRES-GFP) vectors as previously described[12]. All constructs were verified by sequencing. Recombinant proteins FGF2 (8910, Cell Signaling), HGF (100-39, Peprotech), EGF (AF-100-15, Peprotech), and NRG1 (100-03, Peprotech) were used at 50 ng ml^{-1} for 10 min.

Cell culture, compounds, and competitive proliferation assays. H23, H460, H2030, H358, H2122, H820, H3255, and A549 cells were provided by R. Somwar and H. Varmus. H2009, HCT116, SW480, SW620, DLD-1, PaTu 8988t, 3T3, MIAPACA-2, and PANC-1 cells were purchased from the American Type Culture Collection (ATCC). H69, H82, HCC-33, and H446 were provided by C. Rudin. H1975, H1650, Ludlu-1, H1703, PC-14, H2170, SK-MES-1, H520, H522, EBC-1, HCC-15, H441, A-427, and H1299 cells were provided by M. Sanchez-Cespedes. Cell lines were not authenticated. Murine *KRAS*^{G12D}; *p53*^{R270H} cells were derived from a murine lung adenocarcinoma. Cells were maintained in a humidified incubator at 37 °C with 5% CO_2, grown in RPMI 1640 or DMEM supplemented with 10% FBS and 100 IU ml^{-1} penicillin/streptomycin. All cell lines used were negative for mycoplasma.

Trametinib (S2673), SCH772984 (S7101), Gefitinib (S1025), Crizotinib (S1068), CP-724714 (S1167), Afatinib (S1011), BGJ398 (S2183), AZD4547 (S2801), and Ponatinib (S1490) were obtained from Selleckchem. Drugs for *in vitro* studies were dissolved in DMSO to yield 5 or 10 mM stock solutions and stored at −80 °C.

For shRNA experiments, when necessary, human cancer cells were modified to express the ecotropic receptor and rtTA3 by retroviral transduction of MSCV-RIEP (MSCV-rtTA3-IRES-EcoR-PGK-Puro) followed by drug selection (1 μg ml^{-1} puromycin for 1 week). Cell lines were transduced with ecotropically packaged TRMPV-Neo-shRNA retroviruses or, alternatively, with amphotropically packaged LT3GEPIR-Puro-shRNA lentiviruses, selected with 1 mg ml^{-1} G418 or 1 μg ml^{-1} puromycin for 1 week, and treated with 1 μg ml^{-1} doxycycline to induce shRNA expression.

For competitive proliferation assays, shRNA-transduced cells were mixed with non-transduced cells (8:2) and cultured with doxycycline in the presence or absence of trametinib (25 nM). The relative percentage of Venus$^+$/dsRed$^+$ or GFP$^+$ cells was determined before (T_0, blue bars) and after ten population doublings (*Tf*) (results are relative to T_0) (*Tf* on doxycycline, grey bars; *Tf* on dox + trametinib, red bars). The quantification of fluorescent cells was monitored on a Guava Easycyte (Millipore). Experiments were performed independently two or three times.

Lentiviral production. Lentiviruses were produced by co-transfection of 293T cells with lentiviral-Cre backbone construct and packaging and envelope vectors (psPAX2 and VSV-G), using the calcium phosphate method. Supernatant was collected 48, 60, and 72 h after transfection, concentrated by ultracentrifugation at 24,000 r.p.m. for 120 min and resuspended in an appropriate volume of HBSS solution (Gibco).

Clonogenic and apoptosis assay. For clonogenic assays, cells were seeded in triplicate into six-well plates (5×10^3 to 10×10^3 cells per well) and allowed to adhere overnight in regular growth media. Cells were then cultured in the absence or presence of drug as indicated in complete media for 10–14 days. Growth media with or without drug was replaced every 2 days. Remaining cells were fixed with methanol (1%) and formaldehyde (1%), stained with 0.5% crystal violet, and photographed using a digital scanner. Relative growth was quantified by densitometry after extracting crystal violet from the stained cells using 10% of acetic acid. All experiments were performed at least three times. Representative experiments are shown.

For apoptosis assays, around 1×10^6 cells were seeded into 10-cm plates and cultured in the presence or absence of drugs as indicated. After 6 days, apoptosis and cell death were determined using AnnexinV-APC apoptosis detection kit according to the manufacturer's instructions (Affymetrix eBioscience). Data were acquired using a FACS Calibur (BD Biosciences). All experiments were performed independently three times.

Quantitative analysis of drug synergy and determination of fold change in sensitivity to trametinib. Drug synergism was analysed using CompuSyn software (version 1.0) (http://www.combosyn.com), which is based on the median-effect principle (Chou) and the combination index–isobologram theorem (Chou–Talalay)[32]. CompuSyn software generates combination index (CI) values, where CI < 0.75 indicates synergism, CI = 0.75–1.25 indicates additive effects, and CI > 1.25 indicates antagonism. Following the instruction of the software, drug combinations at non-constant ratios were used to calculate the combination index in our study.

For calculating the fold change in sensitivity to trametinib, the concentration of trametinib that inhibited cell proliferation by 50% (GI_{50}) was determined for a panel of KRAS wild-type and mutant cancer cell lines in the absence or presence of ponatinib and AZD4547. Experiments were performed independently twice.

Immunoblotting and RAS-GTP assay. Phospho-lysis buffer (50 mM Tris pH 7.5, 1% Tween-20, 200 mM NaCl, 0.2% NP-40) supplemented with phosphatase inhibitors (5 mM sodium fluoride, 1 mm sodium orthovanadate, 1 mm sodium pyrophosphate, 1 mM β-glycerophosphate), and protease inhibitors (Protease Inhibitor Cocktail Tablets, Roche) was used for cell lysis, and protein concentration was determined by a Bradford protein Assay kit (Biorad). Proteins were separated by SDS-PAGE and immunoblotted and transferred to polyvinyl difluoride (PVDF) membranes (Millipore) according to standard protocols. Membranes were immunoblotted with antibodies against pERK$^{T202/Y204}$ (9101), tERK (9107), pAKT^{S473} (4060), tAKT (9272), pFRS2^{Y436} (3861), pSTAT3^{Y705} (9145), pMEK$^{S217/221}$ (9154), MEK (4694), pMET$^{Y1234/1235}$ (3077), MET (8198), pERBB2$^{Y1221/1222}$ (2243), pEGFR^{Y1068} (3777), EGFR (4267), pERBB3^{Y1289} (4791), and PTEN (9559) from Cell Signaling; CRAF (SC-227) and BRAF (SC-5284) from Santa Cruz Biotechnology; and KRAS (WH0003845M1) from Sigma in 5% BSA in TBS blocking buffer. After primary antibody incubation, membranes were probed with ECL anti-rabbit IgG, anti-mouse IgG or anti-goat IgG secondary antibody (1:10,000) from GE Healthcare Life Science and imaged using a FluorChem M system (protein simple). GTP-bound RAS was measured using a CRAF RAS-binding-domain (RBD) pull down and detection kit (8821, Cell Signaling) as instructed by the manufacturer. All immunoblots were performed independently at least twice.

qRT–PCR. Total RNA was isolated using TRIZOL (Invitrogen), and complementary DNA was obtained using the TaqMan reverse transcription reagents (Applied Biosystems). Real-time PCR was performed in triplicate in three independent experiments using SYBR Green PCR Master Mix (Applied Biosystems) on the

ViiA 7 Real-Time PCR System (Invitrogen). GAPDH or β-actin served as endogenous normalization controls.

Animal studies. All mouse experiments were approved by the Memorial Sloan Kettering Cancer Center (MSKCC) Animal Care and Use Committee (protocol number 12-04-006). Mice were maintained under specific pathogen-free conditions, and food and water were provided *ad libitum*. Female 5- to 7-week-old athymic NCR-NU-NU (Harlan Laboratories) mice were used for animal experiments with human cell lines and patient-derived xenografts. For A549, H23, and H2122 xenografts, cells (10×10^6) were harvested on the day of use and injected in growth-factor-reduced Matrigel/PBS (50% final concentration). One flank was injected subcutaneously per mouse. For JHU-LX55a patient-derived xenograft, a poorly differentiated lung adenocarcinoma bearing a $KRAS^{G12C}$ mutation, tumours were cut into pieces and inserted into a pocket in the subcutaneous space as previously described[33]. After inoculation, mice were monitored daily, weighed twice weekly, and calliper measurements begun when tumours became visible. Tumour volume was calculated using the following formula: tumour volume $= (D \times d^2)/2$, in which D and d refer to the long and short tumour diameter, respectively. When tumours reached a size of 150–300 mm^3, mice were randomized into five to eight per group and treated with vehicle, trametinib, and/or ponatinib *per os* for 4 consecutive days followed by 3 days off treatment, at 3 mg/kg body weight and 30 mg/kg body weight, respectively. No obvious toxicities were observed in the vehicle- or drug-treated animals as assessed by difference in body weight between vehicle- and drug-treated mice taking tumour size into account. For immunohistochemistry analysis of JHU-LX55a patient-derived xenograft tumours, tumours were harvested 4 h after dosing on day 18.

For drug efficacy studies using a GEMM of lung cancer, $Kras^{LSL\text{-}G12D/+}$ and $Trp53^{fl/fl}$ mice (8–12 weeks old) were anaesthetized by intraperitoneal injection of ketamine (80 mg per kg body weight) and xylazine (10 mg per kg body weight) and infected intratracheally with 2.5×10^5 infectious particles of Lenti-Cre per mouse, as previously described[34]. Mice were evaluated by micro-computed tomography imaging to quantify lung tumour burden before being assigned to various treatment study cohorts. Mice were treated with vehicle, trametinib and/or ponatinib *per os* for 4 consecutive days followed by 3 days off treatment, at 3 mg/kg body weight and 30 mg/kg body weight, respectively. Micro-computed tomography imaging evaluation was repeated every week during the treatment. Investigators were not blinded with respect to treatment.

For drug efficacy studies using an organoid-derived murine model of pancreatic cancer, spherical, duct-like organoids were derived and cultured in Matrigel and defined media as previously described[35] from pancreatic ductal adenocarcinoma (PDAC) occurring in $Kras^{LSL\text{-}G12D/+}$; $Trp53^{fl/+}$; *CHC* (untargeted collagen homing cassette); *RIK* (Rosa26-LSL-rtTa3-IRES-Kate2); *p48Cre* mice (GEMM-$KPC^{fl/+}$) generated via the PDAC–GEMM–ESC approach[36]. After initially establishing primary organoid cultures, Kate-positive cells were sorted and expanded to minimize injection of non-recombined, normal duct cells. For the orthotopic transplantation of PDAC organoids, mice were anaesthetized using isoflurane, and the pancreas was externalized through a small incision made in the left abdominal side near the spleen. Organoids (approximately 250,000–500,000 cells per mouse) were removed from Matrigel and separated into single cells by trypsinization, washed, and finally resuspended in 25 μl of Matrigel (BD) diluted 1:1 with cold PBS. The organoid suspension was injected into the tail region of the pancreas using 28-gauge surgical syringes (Hamilton). Successful injection was verified by the appearance of a fluid bubble without signs of intraperitoneal leakage. The abdominal wall was sutured with absorbable Vicryl suture (Ethicon), and the skin was closed with wound clips (CellPoint Scientific). Mice were evaluated by ultrasound (Vevo 2100, VisualSonics) to quantify pancreas tumour burden before being randomized to various treatment study cohorts. All the treatment mice had similar initial tumour burden. Mice were treated as described above for drug efficacy studies using a GEMM of lung cancer. Investigators were not blinded with respect to treatment.

Micro-computed tomography imaging. Micro-computed tomography scans were performed on a Mediso Nano SPECT/CT System covering only the lung fields of each mouse. Each scan averaged approximately 6 min using 240 projections with an exposure time of 1,000 ms set at a pitch of 1°. The tube energy of the X-ray was 55 kVp and 145 μA. The in-plane voxel sizes chosen were small and thin creating a voxel size of 73 μm × 73 μm × 73 μm. The final reconstructed image consisted of 368 voxels × 368 voxels × 1,897 voxels. Scans were analysed with Osirix software.

Patients' samples. Patients with *KRAS* mutation-positive advanced lung adenocarcinomas were enrolled in the phase I/II clinical study of trametinib and navitoclax (NCT02079740) and the response was assessed per RECIST (response evaluation criteria in solid tumours) criteria. Biopsies were obtained before treatment, and within 2–4 weeks after starting the treatment with trametinib. Specifically, for patient 1, the post-treatment biopsy was obtained after treatment with navitoclax for 7 days, followed by co-treatment with navitoclax and trametinib for 16 days. The post-treatment biopsy from patient 2 was obtained after co-treatment with navitoclax and trametinib for 22 days. All human studies were approved by the Massachusetts General Hospital Institutional Review Board, and informed consent to study was obtained as per protocol from all patients.

Immunohistochemistry. Tissues were fixed overnight in 4% paraformaldehyde, embedded in paraffin, and cut into 5 μm sections. Sections were subjected to haematoxylin and eosin staining, and immunohistochemical staining following standard protocols. The following primary antibodies were used: $pERK^{T202/Y204}$ (4370) and $pAKT^{S473}$ (4060) (Cell signaling), and $pFRS2^{Y436}$ (ab193363) (Abcam).

Statistical analysis. Data are expressed as mean ± s.e.m. or mean ± s.d. Group size was determined on the basis of the results of preliminary experiments and no statistical method was used to predetermine sample size. The indicated sample size (n) represents biological replicates. Group allocation and outcome assessment were not performed in a blinded manner. All samples that met proper experimental conditions were included in the analysis. Survival was measured using the Kaplan–Meier method. Statistical significance was determined by Student's t-test, log-rank test, and Pearson's correlation using Prism 6 software (GraphPad Software). Significance was set at $P < 0.05$.

30. Fellmann, C. *et al.* Functional identification of optimized RNAi triggers using a massively parallel sensor assay. *Mol. Cell* **41,** 733–746 (2011).
31. Taylor, J., Schenck, I., Blankenberg, D. & Nekrutenko, A. in *Current Protocols in Bioinformatics* (eds Baxevanis, A. D. *et al.*) Ch. 10, Unit 10.5 (Wiley, 2007).
32. Chou, T. C. Drug combination studies and their synergy quantification using the Chou-Talalay method. *Cancer Res.* **70,** 440–446 (2010).
33. Poirier, J. T. *et al.* DNA methylation in small cell lung cancer defines distinct disease subtypes and correlates with high expression of EZH2. *Oncogene* **34,** 5869–5878 (2015).
34. DuPage, M., Dooley, A. L. & Jacks, T. Conditional mouse lung cancer models using adenoviral or lentiviral delivery of Cre recombinase. *Nature Protocols* **4,** 1064–1072 (2009).
35. Huch, M. *et al.* Unlimited in vitro expansion of adult bi-potent pancreas progenitors through the Lgr5/R-spondin axis. *EMBO J.* **32,** 2708–2721 (2013).
36. Saborowski, M. *et al.* A modular and flexible ESC-based mouse model of pancreatic cancer. *Genes Dev.* **28,** 85–97 (2014).

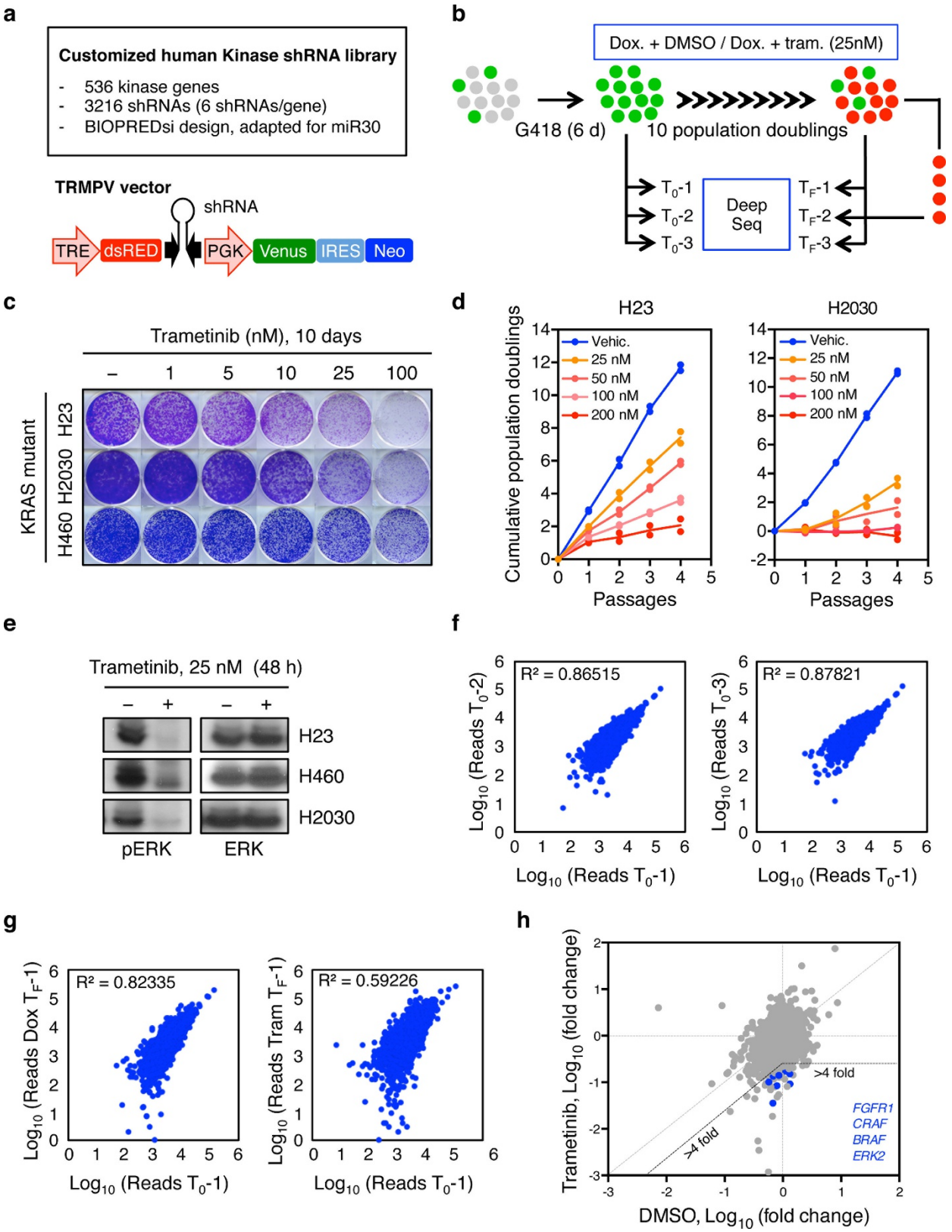

Extended Data Figure 1 | A synthetic lethal RNA interference screen identifies different MAPK signalling effectors and FGFR1 as sensitizers to MEK inhibition in KRAS-mutant lung cancer cells. a, Library features and schematic of the TRMPV-Neo vector. **b**, Schematic outline of the synthetic lethal RNA interference screen for identifying sensitizers to trametinib in KRAS-mutant lung cancer cells. **c**, Clonogenic assay of KRAS-mutant lung cancer cell lines (H23, H460, and H2030) cultured in the presence of increasing concentrations of trametinib. **d**, Proliferation assay of H23 and H2030 cells in the presence of increasing concentrations of trametinib for four passages. Data presented as mean of two independent replicates. **e**, Immunoblot analysis of KRAS-mutant lung cancer cell lines treated with 25 nM of trametinib for 48 h. **f**, **g**, Scatter plots illustrating the correlation of normalized reads per shRNA between replicates at the beginning of the experiment (**d**) and replicates at different time points in the absence (left) or presence (right) of trametinib (25 nM) (**e**). **h**, Scatter plot illustrating the fold change in the relative abundance of each shRNA in the library after ten population doublings on doxycycline in the absence or presence of trametinib (25 nM) in H23 cells. Two shRNAs for *FGFR1*, *CRAF*, *BRAF*, and *ERK2* were identified as selectively depleted in trametinib-treated cells. For gel source data, see Supplementary Fig. 1.

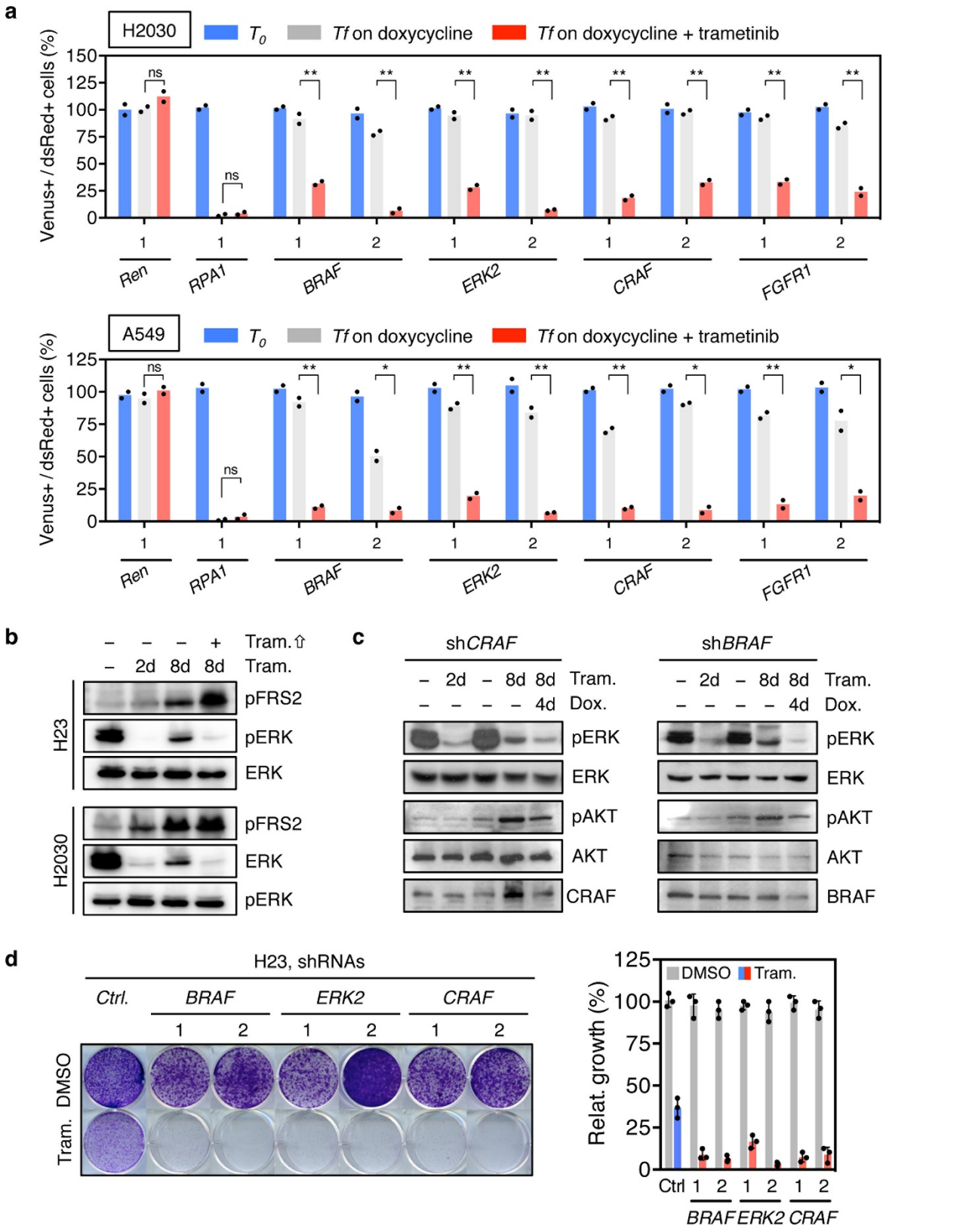

Extended Data Figure 2 | Suppression of FGFR1 and different MAPK signalling effectors reduces the proliferation and viability of KRAS-mutant lung cancer cells treated with trametinib. a, Quantification of fluorescent cells in competitive proliferation assays in H2030 (upper) and A549 (lower) cells transduced with non-targeting control (*Ren*) or the indicated shRNAs. Data presented as mean ($n = 2$). Unpaired two-tailed *t*-test. $^*P < 0.05$, $^{**}P < 0.01$. **b**, Immunoblot of H23 and H2030 cells pre-treated with 25 nM trametinib for various times and subsequently treated with 200 nM trametinib for 2 h. **c**, Immunoblot of H23 cells transduced with doxycycline-inducible shRNAs targeting *CRAF* and *BRAF* and treated with trametinib (25 nM) and doxycycline for the times shown. H23 cells were pre-treated with trametinib for 4 days, followed by treatment with doxycycline and trametinib for 4 days. **d**, Clonogenic assay of H23 cells transduced with *BRAF*, *CRAF*, *ERK2*, and non-targeting control shRNAs, and cultured with DMSO or trametinib (25 nM) for 10 days. Relative growth of DMSO- (grey bars) and trametinib-treated cells (blue and red bars) is shown (right). Data presented as mean ± s.d. ($n = 3$). For gel source data, see Supplementary Fig. 1.

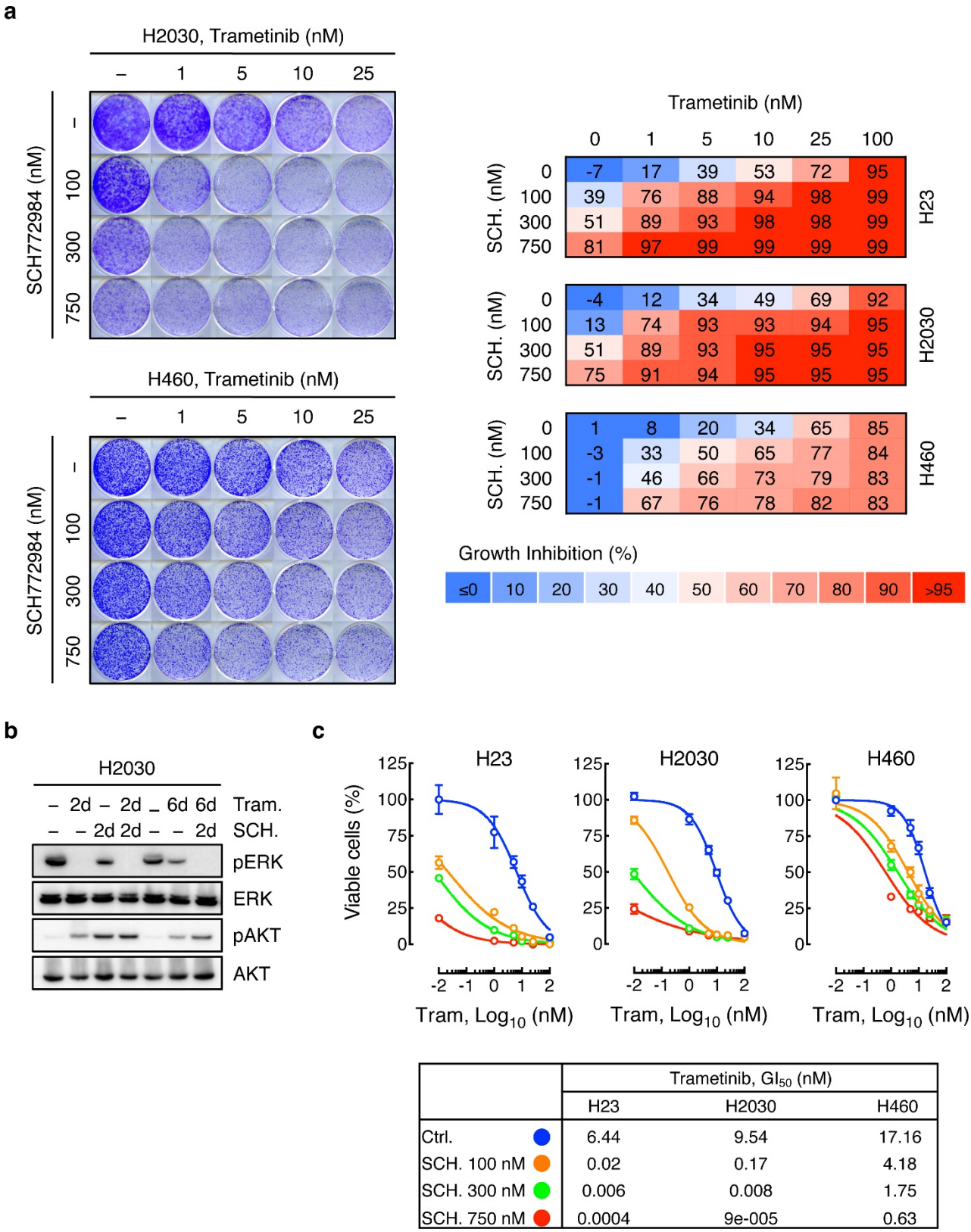

	Trametinib, GI_{50} (nM)		
	H23	H2030	H460
Ctrl.	6.44	9.54	17.16
SCH. 100 nM	0.02	0.17	4.18
SCH. 300 nM	0.006	0.008	1.75
SCH. 750 nM	0.0004	9e-005	0.63

Extended Data Figure 3 | ERK inhibitor SCH772984 enhances the antiproliferative effects of trametinib in KRAS-mutant lung cancer cells. a, Clonogenic assay of H2030 (upper) and H460 (lower) cells treated with increasing concentrations of trametinib, ERK inhibitor SCH772984, or their combination as indicated. Percentage inhibition at each concentration of the drugs in H23, H2030, and H460 cells is presented (right). Data presented as mean of three independent experiments ($n = 3$). **b**, Immunoblot analysis of H2030 cells treated with trametinib (25 nM), SCH772984 (500 nM), or their combination for the times shown. H2030 cells were pre-treated with trametinib for 4 days, followed by treatment with SCH772984 and trametinib for 2 days. **c**, Cell viability of H23, H2030, and H460 cells treated with increasing doses of trametinib, ERK inhibitor SCH772984, or their combination for 10 days. Data presented as mean ± s.d. ($n = 3$). The GI_{50} was calculated in the absence or the presence of increasing concentrations of SCH772984 (bottom). For gel source data, see Supplementary Fig. 1. Source Data for Extended Data Fig. 3 are available in the online version of the paper.

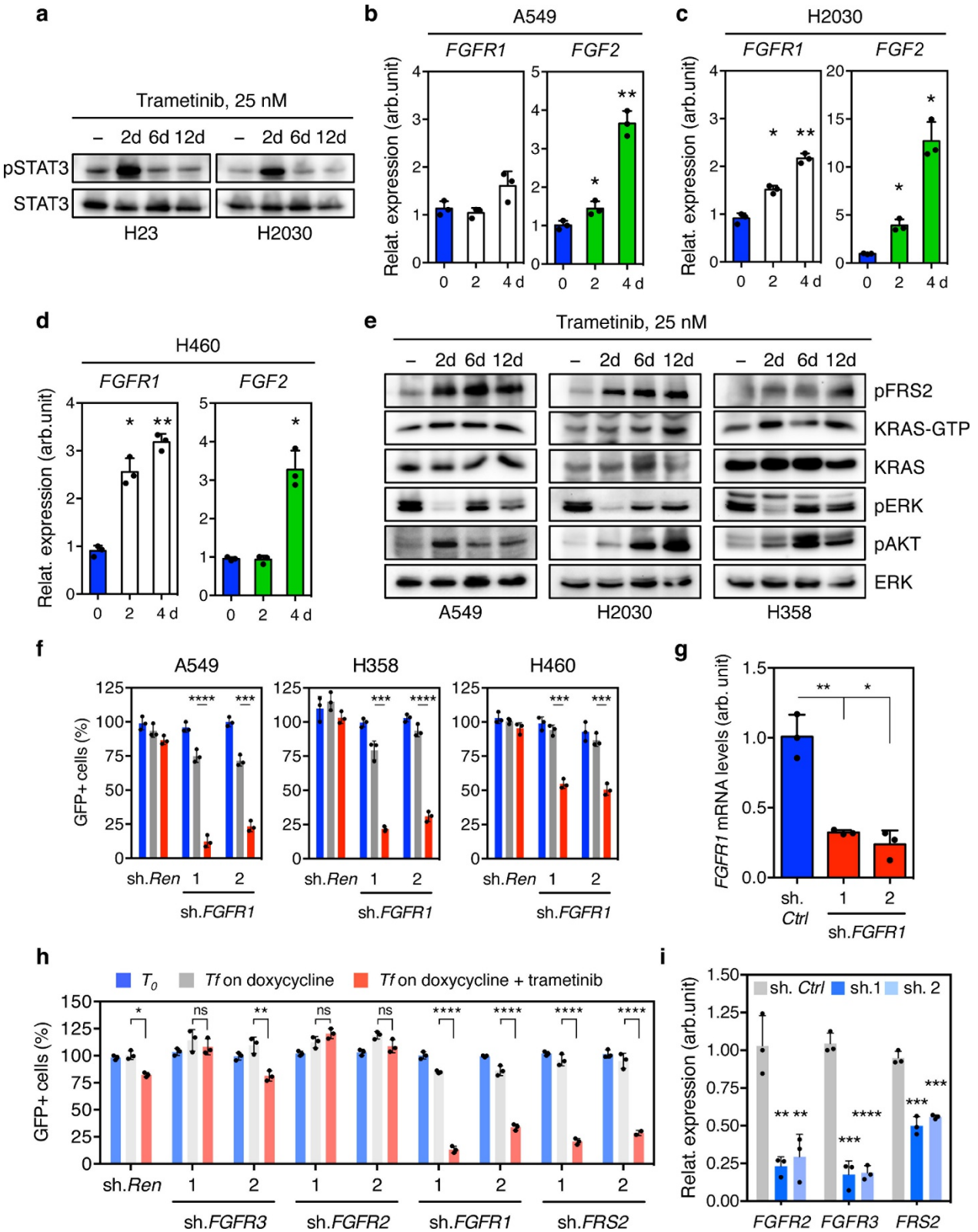

Extended Data Figure 4 | Feedback activation of FGFR1 signalling leads to adaptive resistance to trametinib in KRAS-mutant lung cancer cells. **a**, Immunoblot analysis of KRAS-mutant lung cancer cell lines H23 and H2030 treated with 25 nM trametinib for various times. **b**–**d**, qRT–PCR for *FGFR1* and *FGF2* in A549 (**b**), H2030 (**c**), and H460 (**d**) cells treated with trametinib for the indicated times. Data presented as mean normalized for *FGFR1* and *FGF2* expression ± s.d. ($n = 3$). **e**, Immunoblot analysis of A549, H2030, and H358 cells treated with trametinib (25 nM) for various times. **f**, Quantification of fluorescent cells in competitive proliferation assays in A549, H358, and H460 cells transduced with doxycycline-inducible non-targeting control (*Ren*) or *FGFR1* shRNAs. Data presented as mean ± s.d. ($n = 3$). **g**, qRT–PCR for *FGFR1* in H23 cells transduced with non-targeting control and *FGFR1* shRNAs. Data presented as mean normalized for *FGFR1* expression ± s.d. ($n = 3$). **h**, Quantification of fluorescent cells in competitive proliferation assays in A549 cells transduced with non-targeting control (*Ren*) or the indicated shRNAs. Data presented as mean ± s.d. ($n = 3$). **i**, qRT–PCR for *FGFR2*, *FGFR3*, and *FRS2* in A549 cells transduced with non-targeting control, *FGFR2*, *FGFR3*, and *FRS2* shRNAs. Data presented as mean normalized for *FGFR2*, *FGFR3*, and *FRS2* expression ± s.d. ($n = 3$). **b**–**d**, Paired two-tailed *t*-test. **f**–**i**, Unpaired two-tailed *t*-test. $^{*}P < 0.05$, $^{**}P < 0.01$, $^{***}P < 0.001$, $^{****}P < 0.0001$. For gel source data, see Supplementary Fig. 1.

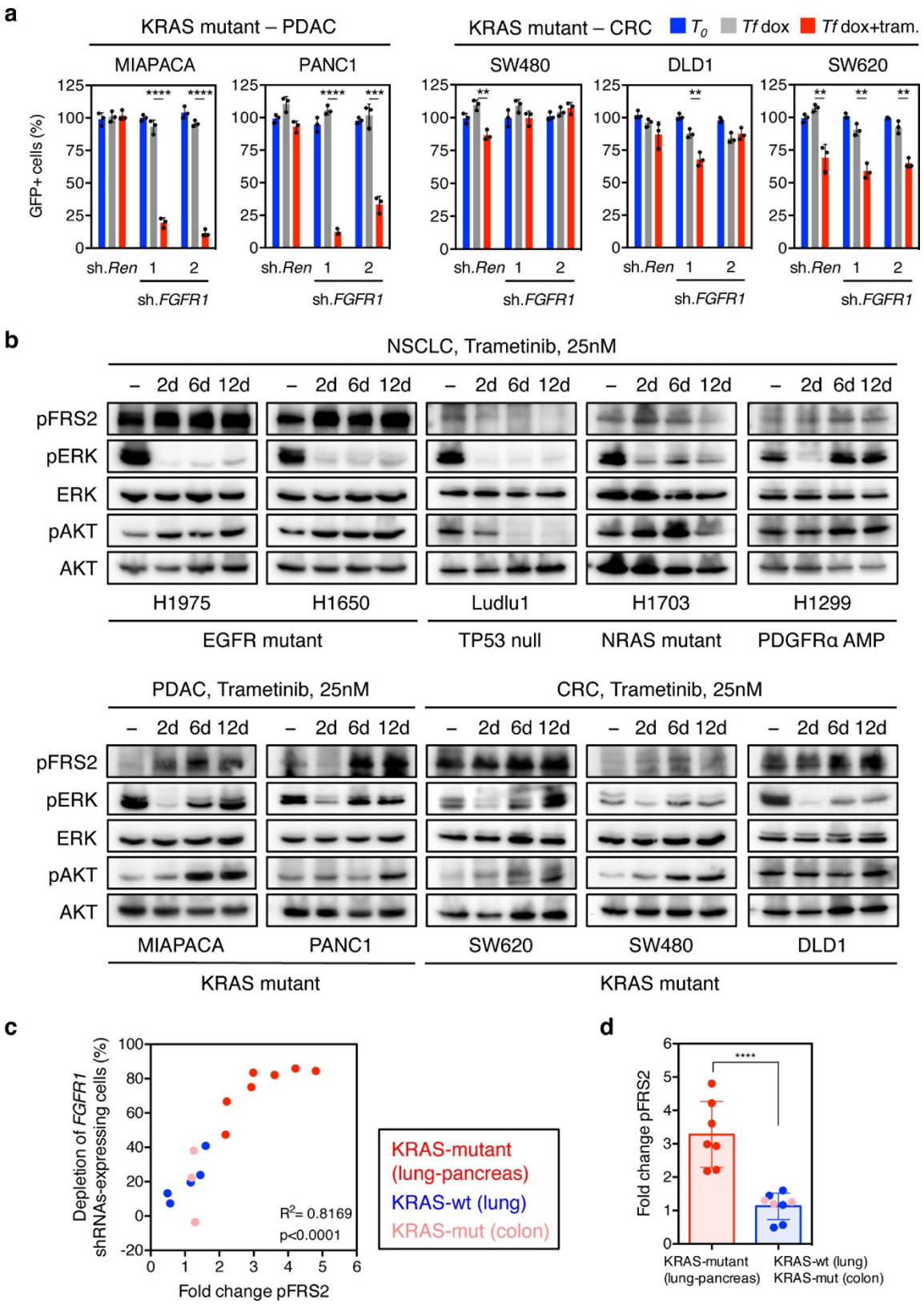

Extended Data Figure 5 | Trametinib-induced phosphorylation of FRS2 predicts sensitivity to MEK and FGFR1 combined inhibition. **a**, Competitive proliferation assays in the indicated KRAS-mutant cancer cell lines transduced with doxycycline-inducible non-targeting control (*Ren*) or *FGFR1* shRNAs. Data presented as mean ± s.d. ($n = 3$). **b**, A panel of lung (H1975, H1650, Ludlu-1, H1703, and H1299), pancreas (MIAPACA, PANC1), and colorectal (SW620, SW480, and DLD1) cancer cell lines were treated with 25 nM trametinib for various times. Lysates were subject to immunoblot analysis with the indicated antibodies. **c**, Scatter plot illustrating the correlation between depletion of *FGFR1* shRNAs-expressing cells and fold change in FRS2 phosphorylation after trametinib treatment in human cancer cells lines ($n = 15$). **d**, Representation of the fold change in FRS2 phosphorylation after treatment with trametinib for 12 days in human cancer cell lines ($n = 15$). **a**, **d**, Unpaired two-tailed *t*-test. **c**, Two-tailed Pearson's correlation. $^{**}P < 0.01$, $^{***}P < 0.001$, $^{****}P < 0.0001$. For gel source data, see Supplementary Fig. 1.

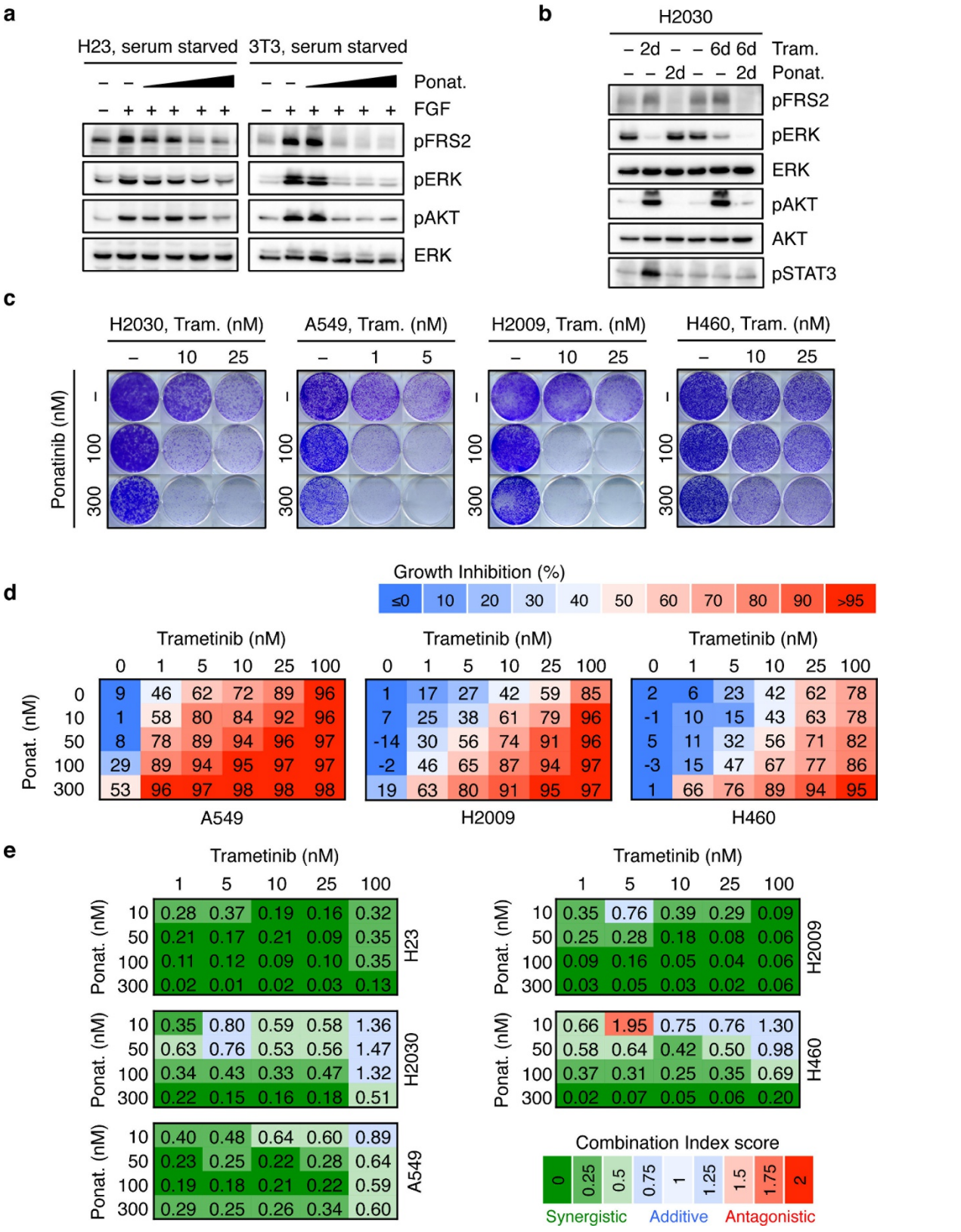

Extended Data Figure 6 | Trametinib in combination with ponatinib synergizes at inhibiting cell proliferation of KRAS-mutant lung cancer cells. a, Serum starved H23 (left) and 3T3 (right) cells were pre-treated with increasing concentration of ponatinib for 24 h (1, 30, 100, and 300 nM), followed by stimulation with FGF2 (50 ng ml^{-1}) for 10 min. Immunoblot analysis for the indicated antibodies is shown. **b**, Immunoblot analysis of H2030 cells treated with trametinib (25 nM), ponatinib (750 nM), or their combination for the times shown. Cells were pre-treated with trametinib for 4 days, followed by co-treatment with ponatinib and trametinib for 2 days. **c**, Clonogenic assay of H2030, A549, H2009, and H460 cells treated with increasing concentrations of trametinib, ponatinib, or their combination as indicated. **d**, Percentage of cell growth inhibition at each concentration of trametinib, ponatinib, or their combination in A549, H2009, and H460 cells after is shown. Data presented as mean of three independent experiments ($n = 3$). **e**, Combination index (CI) scores for H23, H2030, A549, H2009, and H460 cells treated with trametinib in combination with ponatinib at the indicated concentrations. Each CI score represents data from at least three independent experiments. For gel source data, see Supplementary Fig. 1. Source Data for Extended Data Fig. 6 in the online version of the paper.

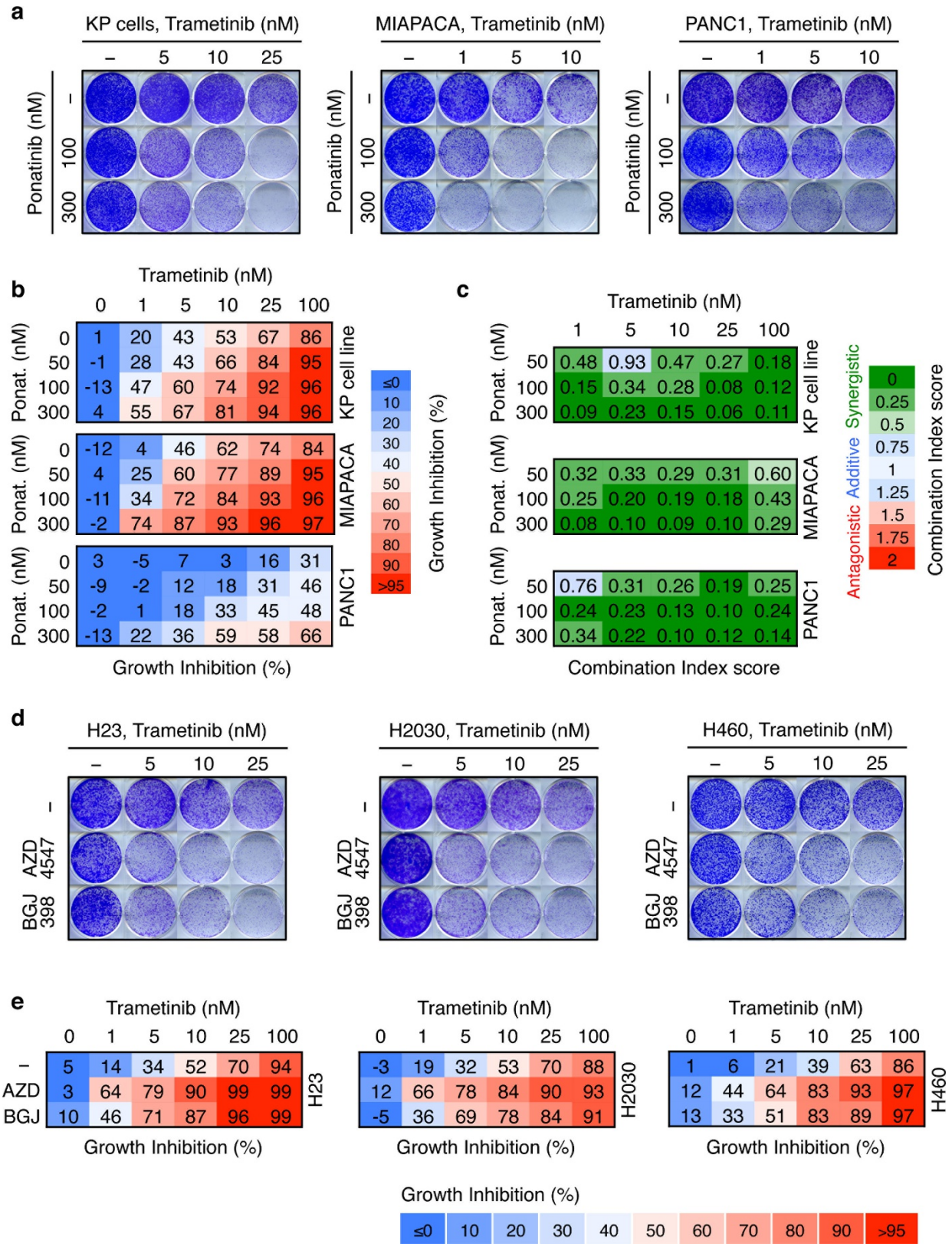

Extended Data Figure 7 | Distinct FGFR1 inhibitors sensitize murine and human KRAS-mutant cancer cells to trametinib. a, Clonogenic assay of a murine lung cancer cell line harbouring $Kras^{G12D}$ and $Trp53^{R270H}$ mutations (KP cell line), and human KRAS-mutant pancreatic cancer cell lines (MIAPACA and PANC1). Tumour cells were cultured with increasing concentrations of trametinib, ponatinib, or their combination as indicated. **b**, Percentage of cell growth inhibition at each concentration of trametinib, ponatinib, or their combination in KP, MIAPACA, and PANC1 cells is shown. Data presented as mean of three independent replicates ($n = 3$). **c**, Combination index scores for KP, MIAPACA, and PANC1 cells treated with trametinib in combination with ponatinib at the indicated concentrations. Each combination index score represents data from at least three independent experiments ($n = 3$). **d**, Clonogenic assay of H23, H2030, and H460 cells cultured with increasing concentrations of trametinib alone or in combination with FGFR1 inhibitors BGJ398 (1.5 μM) or AZD4547 (2 μM). **e**, Percentage of cell growth inhibition at each concentration of trametinib alone or in combination with BGJ398 (1.5 μM) or AZD4547 (2 μM) in H23, H2030, and H460 cells is shown. Data presented as mean of three independent replicates ($n = 3$). Source Data for Extended Data Fig. 7 is available in the online version of the paper

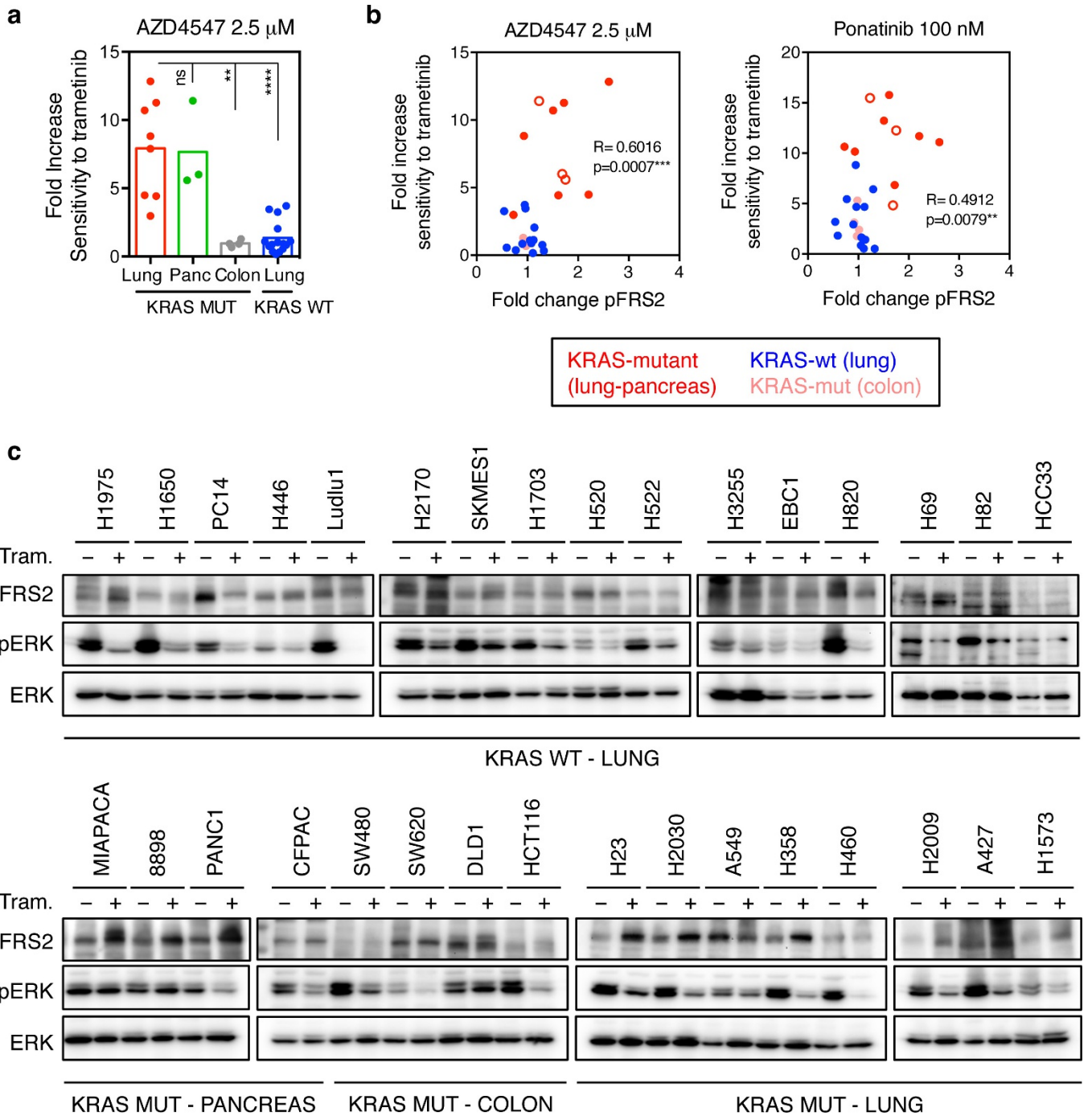

Extended Data Figure 8 | The magnitude of trametinib-induced FRS2 phosphorylation correlates with the sensitivity to trametinib and FGFR1 combined inhibition in human cancer cells. a, Dot plot illustrating the sensitivity increase to trametinib after the treatment with AZD4547 (2.5 μM) in a panel of KRAS-mutant ($n = 15$) and KRAS wild-type ($n = 15$) cancer cell lines. Data presented as mean of two independent replicates ($n = 2$). **b**, Scatter plot illustrating the correlation between fold increase in sensitivity to trametinib after treatment with AZD4547 (2.5 μM) or ponatinib (100 nM) and fold change in FRS2 phosphorylation after trametinib treatment in a panel of human cancer cells lines. **c**, Immunoblot analysis of a panel of human cancer cells treated with trametinib (25 nM) for 6 days. **a**, Unpaired two-tailed *t*-test. **b**, Two-tailed Pearson's correlation. $^{**}P < 0.01$, $^{***}P < 0.001$, $^{****}P < 0.0001$. For gel source data, see Supplementary Fig. 1.

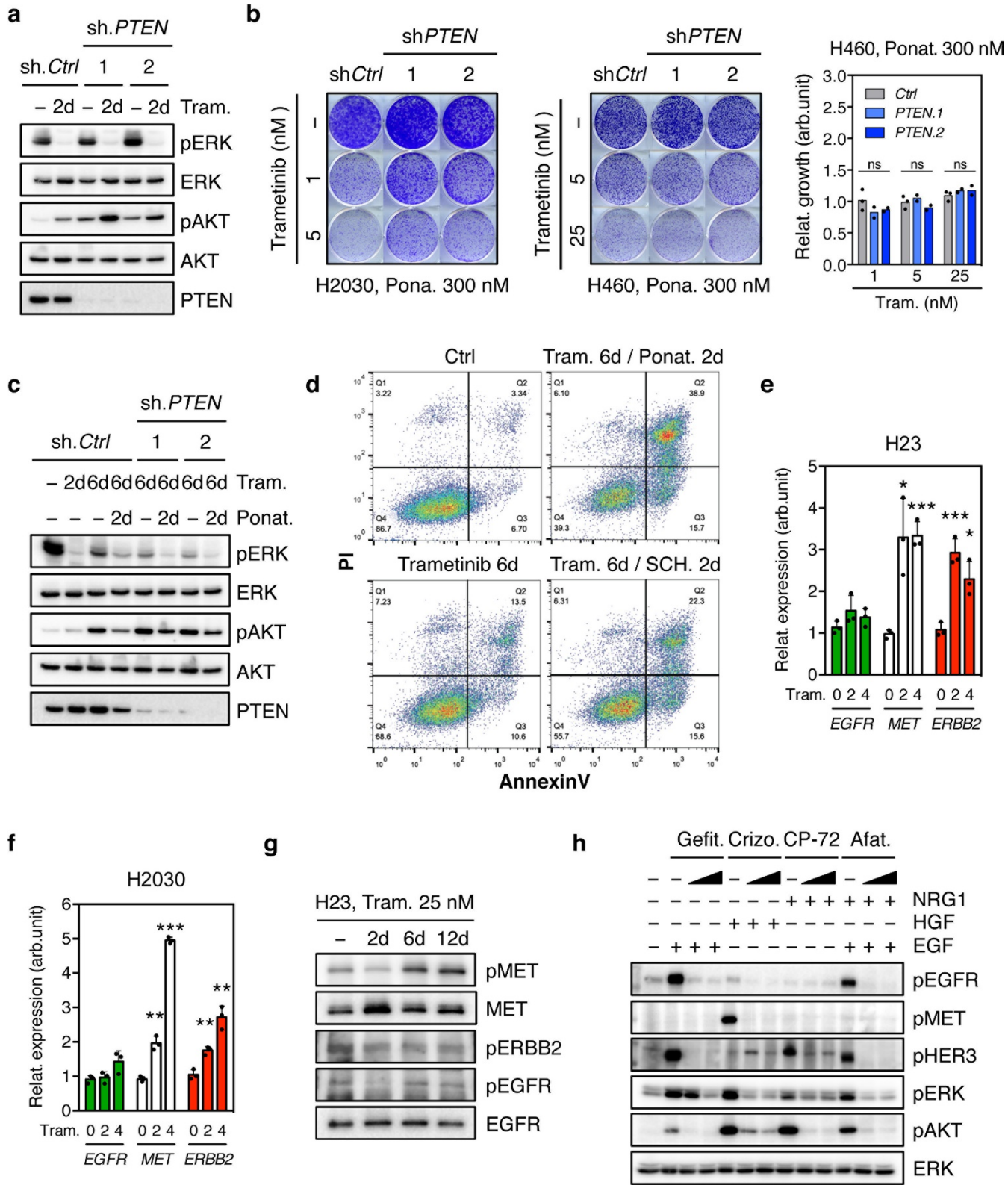

Extended Data Figure 9 | See next page for caption.

Extended Data Figure 9 | Ponatinib prevents trametinib-induced reactivation of MAPK and PI3K signalling. Upregulation of distinct RTKs in KRAS-mutant lung cancer cells after trametinib treatment. **a**, Immunoblot analysis of H2030 transduced with *PTEN* and non-targeting control shRNAs, and treated with trametinib (25 nM) for the times shown. **b**, Clonogenic assay of H2030 (left) and H460 (middle) cells transduced with *PTEN* and non-targeting control shRNAs. Cells were treated with ponatinib alone (300 nM) or in combination with trametinib at the indicated concentrations. Quantification of the relative cell growth of H460 cells is shown (right). Data presented as mean of two independent experiments. **c**, Immunoblot analysis of H2030 transduced with *PTEN* and non-targeting control shRNAs, and treated with trametinib (25 nM) alone or in combination with ponatinib (750 nM) for the times shown. PTEN suppression did not affect ERK signalling or its inhibition after trametinib treatment but instead activated AKT and, more importantly, attenuated the ability of ponatinib to suppress trametinib-induced increase in pAKT. **d**, AnnexinV/PI double staining assay of H23 cells treated with vehicle, trametinib (25 nM) alone or in combination with ponatinib (300 nM) or SCH772984 (1 μM) for the times shown ($n = 3$). **e**, **f**, qRT–PCR for *EGFR*, *MET*, and *ERBB2* in H23 (**e**) and H2030 (**f**) cells treated with trametinib for 0, 2, and 4 days. Data presented as mean normalized for *EGFR*, *MET*, and *ERBB2* expression ± s.d. ($n = 3$). **g**, Immunoblot analysis of H23 cells treated with 25 nM of trametinib for various times. **h**, Immunoblot analysis of serum starved H2030 cells pre-treated with 500 nM or 1 μM of gefitinib, crizotinib, CP-724714, or afatinib for 12 h, followed by stimulation with EGF, HGF, NRG1, or their combination (50 ng ml^{-1}) for 10 min. **b**, **e**, **f**, Unpaired two-tailed *t*-test. *$P < 0.05$, **$P < 0.01$, ***$P < 0.001$. For gel source data, see Supplementary Fig. 1.

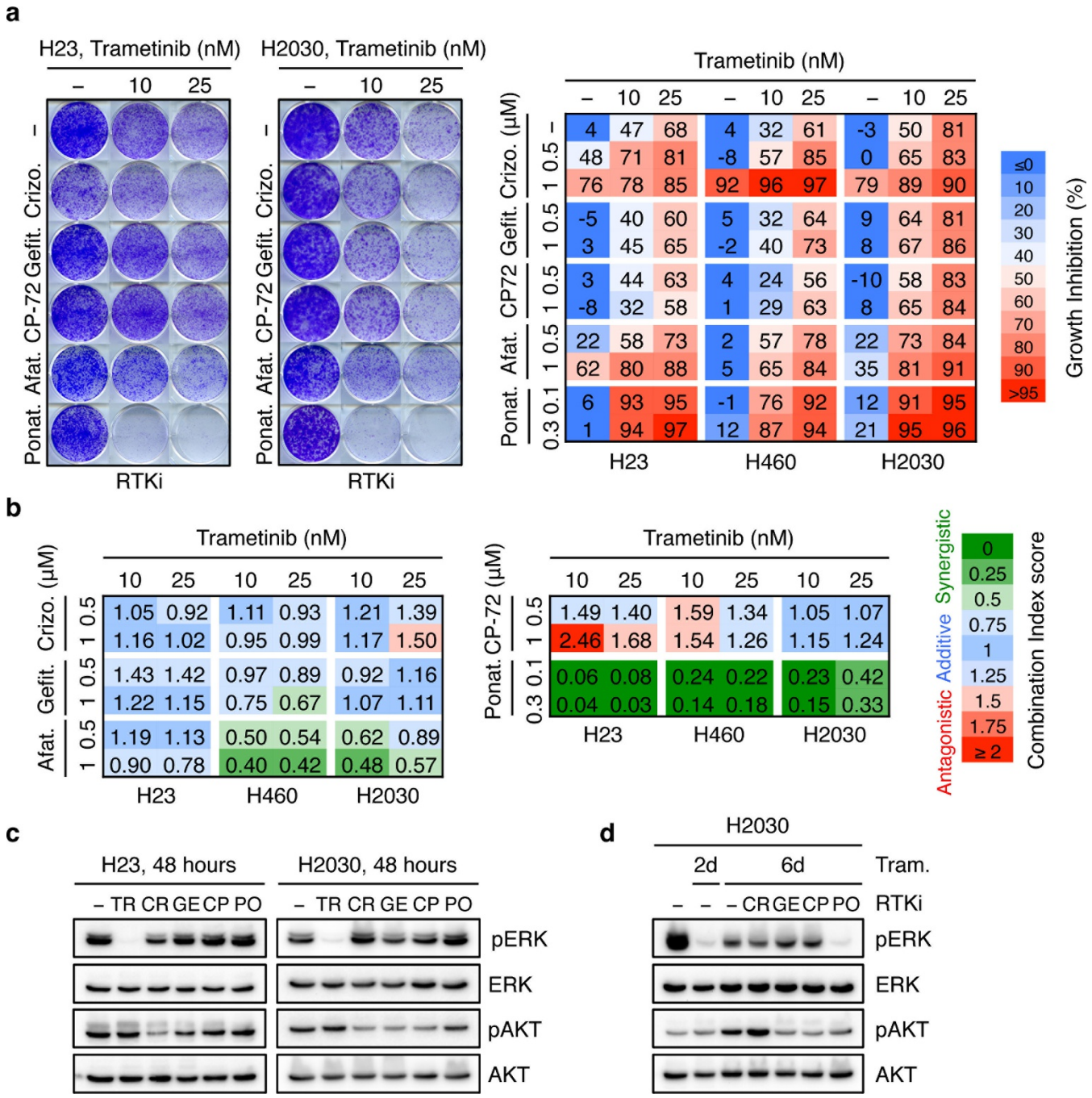

Extended Data Figure 10 | Unresponsiveness of KRAS-mutant lung cancer cells to MEK inhibitor trametinib is predominantly mediated by feedback activation of FGFR1 signalling. a, Clonogenic assay of H23 and H2030 cells treated with increasing concentration of trametinib alone or in combination with 500 nM crizotinib, gefitinib, CP-724714, and afatinib, or 300 nM ponatinib. Percentage inhibition at each concentration of the drugs in H23, H460, and H2030 cells is presented (right). Data presented as mean of at least two independent experiments ($n = 2$). **b**, CI (combination index) scores for H23, H460, and H23 cells treated with trametinib in combination with crizotinib, gefitinib, CP-724714, afatinib, and ponatinib at the indicated concentrations. Each CI score represents data from at least two independent experiments ($n = 2$). **c**, Immunoblot of H23 and H2030 treated with trametinib (25 nM), crizotinib (1 μM), gefitinib (1 μM), CP-724714 (1 μM), and ponatinib (750 nM) for 48 h. **d**, Immunoblot analysis of H2030 treated with trametinib (25 nM), crizotinib (1 μM), gefitinib (1 μM), CP-724714 (1 μM), ponatinib (750 nM), or their combination for the times shown. Cells were pre-treated with trametinib for 4 days, followed by co-treatment with RTK inhibitors and trametinib for 2 days. For gel source data, see Supplementary Fig. 1. Source Data for Extended Data Fig. 10 are available in the online version of this paper.

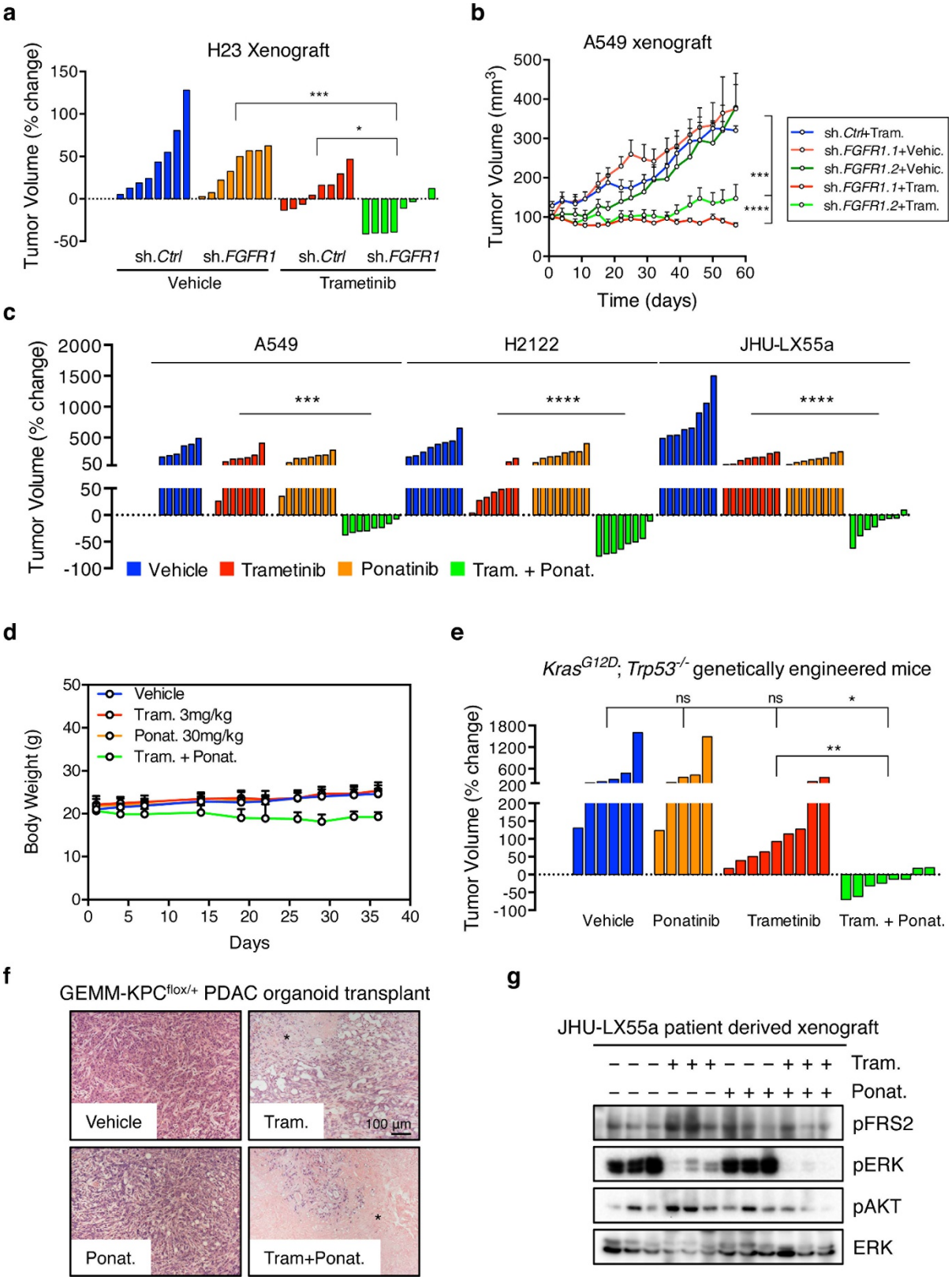

Extended Data Figure 11 | See next page for caption.

Extended Data Figure 11 | Suppression of FGFR1 cooperates with trametinib to inhibit growth of KRAS-mutant lung tumours. a, **b**, Mice bearing H23 (**a**) or H2030 (**b**) xenografts transduced with *FGFR1* or non-targeting control shRNAs were treated with either vehicle or trametinib (3 mg/kg body weight). For H23 xenografts, a waterfall representation of the best response for each tumour is shown ($n = 8$ per group) (**a**). For H2030 xenografts, the tumour volumes are shown as a function of time after treatment. Error bars, mean ± s.e.m. ($n \geq 4$ per group) (**b**). **c**, Mice bearing A549 and H2122 xenografts, and JHU-LX55a patient-derived xenograft tumours were treated with vehicle, trametinib (3 mg/kg body weight), ponatinib (30 mg/kg body weight), or both drugs in combination. A waterfall representation of the best response for each tumour is shown ($n \geq 6$ per group). **d**, Body weight of mice bearing A549 xenografts and treated with vehicle, trametinib (3 mg/kg body weight), ponatinib (30 mg/kg body weight), or both drugs in combination for the indicated times ($n \geq 6$ per group). **e**, $Kras^{G12D}$; $Trp53^{-/-}$ genetically engineered mice harbouring lung adenocarcinomas were treated with vehicle, trametinib (3 mg/kg body weight), ponatinib (30 mg/kg body weight), or both drugs in combination for 7 weeks. A waterfall representation of the response for each tumour after 7 weeks of treatment is shown ($n \geq 5$). **f**, Representative haematoxylin and eosin stains of pancreatic tumour tissue resulting from orthotopic transplantation of GEMM-$KPC^{flox/+}$ PDAC organoids. Mice were treated with vehicle, trametinib (3 mg/kg body weight), ponatinib (30 mg/kg body weight), or both drugs in combination. Black asterisk indicates necrosis. **g**, Immunoblot analysis of tumour tissue from mice bearing JHU-LX55a patient-derived xenografts treated with vehicle, trametinib (3 mg/kg body weight), ponatinib (30 mg/kg body weight), or both drugs in combination for 18 days. **a**–**c**, **e**, Unpaired two-tailed *t*-test. $^{*}P < 0.05$, $^{**}P < 0.01$, $^{***}P < 0.001$, $^{****}P < 0.0001$. For gel source data, see Supplementary Fig. 1. Source Data for Extended Data Fig. 11 are available in the online version of this paper.